Bulletin of the New Zealand Society for Earthquake Engineering, Vol. 56, No. 2, June 2023

PERFORMANCE OF ROCKING FRAMES WITH FRICTION TENSION-ONLY DEVICES

Kiran Rangwani[1], Gregory MacRae[2] and Geoffrey Rodgers[3]

(Submitted *December 2021*; Reviewed *May 2022*; Accepted *August 2022*)

ABSTRACT

The implementation of a new friction tension-only "GripNGrab" device attached to a rocking steel frame is described. The device, when subject to significant tension dissipates energy via sliding in the frictional component. When the device is loaded in the compression direction, almost no compressive force is carried, but displacement occurs in the ratchetting component. This absence of any significant compressive force within the dissipative system means that the rocking frame will always recentre after uplift from earthquake shaking. A 9 m tall 4.75m wide 3-storey steel concentrically braced rocking frame is designed for low-damage seismic performance. Restoring forces are provided by (i) gravity, (ii) friction "GripNGrab" (GNG) tension-only dissipation devices at the base, and (iii) beam-slab effects. The initial fundamental period of the structure was 0.16s. The initial structure used a 10mm GNG ratchet pitch, and had a GNG strength to not slide under serviceability level shaking. Elastic, pushover, cyclic pushover, as well as time history analyses, with different shaking intensities are conducted using OpenSEES software. The scope of work is limited to a single building and a single ground motion. Parameters varied included the presence of beam-slab effects, and the GNG device stiffness, strength and tooth pitch.

It is shown that the full behaviour of the frame could be understood considering cyclic pushover analysis. The peak uplift displacement was conservatively estimated from the peak roof displacement using rigid body mechanics and the tension-only device provided no resistance to full frame recentring. For the frames considered, cumulative uplift displacements, necessary to determine the inelastic displacement capacity of the tension only device, were up to 28 times the peak uplift displacement, not necessarily occurring at the maximum shaking intensity. Maximum frame base shear force demands were up to 1.43 times that from pushover analysis. When the beam-slab, connecting the rocking frame to the rest of the structure, increased the lateral force resistance, the base shear increased significantly, reduced peak roof displacements, and increased the effective number of peak uplift displacement cycles (N_{PUDc}). For large shaking intensities, yielding of the beam-slab occurred resulting in permanent peak roof and uplift displacements. The GNG device strength, stiffness and tooth pitch variations for the cases studied did not significantly affect the response. Initial stiffness, and secant stiffness, based methods to predict the response of rocking frames were non-conservative for these short-period structures with small energy dissipation, and a simple improvement to match the behaviour was developed for the case studied based on the *R*-*T*-μ relationship for a range of shaking intensity.

https://doi.org/10.5459/bnzsee.1583

INTRODUCTION

It is desirable that structures do not need to be extensively repaired or replaced after a major earthquake event. A number of methods have been proposed to increase the resilience of building structures, and therefore increase their seismic sustainability.

One way to increase the resilience is to use structural systems where rocking frames resist the majority of the lateral force. A number of such structures have now been constructed around the world.

To prevent large displacements in rocking frames due to resonance, energy dissipation devices, such as tension-compression dissipaters have been used to reduce the displacements.

However, if large amounts of dissipation are used, then there is a possibility that a rocking structure will not return to its at-rest position after a major earthquake event due to residual compression forces in the energy dissipation devices. In such circumstances, significant additional post-tensioning may be required. Furthermore, it is possible that some tension/compression devices may buckle in compression, especially under the combination of in-plane, and out-of-plane, action.

Recently tension-only devices have been proposed which guarantee that a structure will return to its initial at-rest position, and they eliminate the possibility of buckling. The total deformation of the tension-only dissipaters is dependent only on the number of cycles and amplitude of tension movements during wall uplift.

The energy dissipation component of tension-only devices may be due to yielding or some other means. Many yielding devices have limited deformation capacity due to the fracture strain of steel. Friction devices can provide large inelastic displacement capacities.

However, while tension-only dissipater strengths may satisfy current minimum recommendations to satisfy frame serviceability and wind resistance criteria. The hysteretic energy dissipated is smaller than that of a compression-tension

[1] *Corresponding Author, PhD Candidate, University of Canterbury, Christchurch, kiran.rangwani@pg.canterbury.ac.nz (Student Member)*
[2] *Professor, University of Canterbury, Christchurch, gregory.macrae@canterbury.ac.nz (Fellow)*
[3] *Professor, University of Canterbury, Christchurch, geoff.rodgers@canterbury.ac.nz (Fellow)*

device designed with the same yield force, so the frame displacements may increase. Also, as the displacement capacity of the devices need to accommodate the total cumulative tensile displacement, a sufficient length should be provided to provide the desirable dissipation with sufficient inelastic displacement capacity.

Based on the above discussion, it may be seen that there is a need to quantify how a friction tension-only device is likely to affect the frame performance, and also to obtain the likely frame and device maximum and cumulative inelastic displacement demands so that design may be undertaken with confidence.

This paper seeks to address the needs above by explaining the detailed performance and aspects of one such frame considering an earthquake record scaled to different levels. In particular, answers are sought to the following questions for a 3-storey frame to understand the way that it responds to ground shaking:

1. Is it possible to design a 3-D rocking frame system which has no resistance to self-centring, and which also dissipates significant frictional energy?
2. What can we learn from the cyclic push-pull analysis of the frame?
3. From time history analysis, what are the roof, peak uplift, and cumulative uplift, displacements, and base shear demands?
4. What are the effects of shaking intensity on a frame considering uplift resistance from beam-slabs connected to the gravity frames?
5. How does the frame performance with uplift resistance from beam-slabs connected to the gravity frames compare to that without consideration of these beam-slab effects?
6. What is the sensitivity of the response to tooth pitch and GNG stiffness/strength?
7. Can peak roof displacements be predicted?

PREVIOUS STUDIES

Steel Rocking Frames

The early work on the response of rocking structures was conducted by Housner [1]. Clough and Huckelbridge [2] conducted some of the earliest rocking frame (experimental) tests and compared them with a conventional pin-base (steel) frame. They found that the member forces and floor accelerations of the rocking frame were lower than that of the conventional steel frame. Priestley et al. [3] developed a simple method to evaluate the rocking response of structures via the displacement response spectra using the equivalent damping of the rocking system. The earliest world leading application of rocking solutions was in 1981 on bridge piers of South Rangitikei Rail Bridge in New Zealand (NZ) [4,5] and on elevated freeway bridges in 1992 by Xiao et al. [6].

Rocking frames have been recently used in building structures (e.g., [7-9]). In NZ, the first steel structure designed to rock was built in Wellington in 2007 [7]. The rocking elements may be constructed of structural forms (e.g., walls or braced frames), using materials such as concrete, timber or steel. These elements generally uplift at their bases from their foundation and have some sort of key to transfer base shear and prevent wall-sliding at the base [10-16]. The elements are generally designed to remain essentially elastic during an earthquake event. Their lateral force resistance may be a result of gravity as shown in Figure 1(a), plus external post-tensioning using cables over the height of the structure [13] as shown in Figure 1(b), or springs at the base of the structure as shown Figure 1(c) [17], plus effects from the rest of the structure (here referred to as beam-slab effects) as shown Figure 1(d).

To reduce the possibility of frame resonance during earthquake shaking, and to further increase lateral strength, energy dissipation devices, such as those shown in Figure 1(e), may be used. These may be dissipaters like mini buckling restrained braces (BRBs) [18,19], ring-feder springs [17], lead extrusion devices [20,21], symmetrical or asymmetrical frictional devices [22], or others [23]. If one or more of these dissipaters are provided, then there needs to be sufficient energy dissipated for them to be effective, but not too much that they reduce the possibility of self-centring or prevent uplift/rocking.

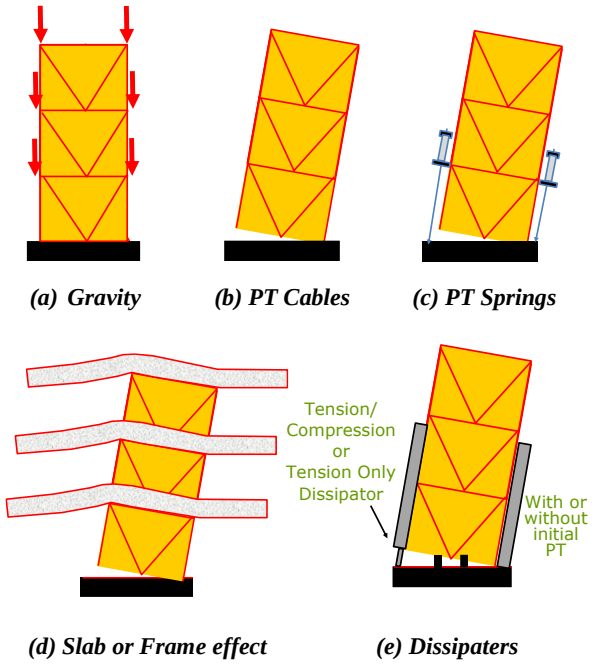

(a) Gravity *(b) PT Cables* *(c) PT Springs*

(d) Slab or Frame effect *(e) Dissipaters*

Figure 1: Rocking frame restoring forces [24].

Midorikawa et al. [25,26] conducted shaking table tests of a half-scale three-story steel rocking frame after installing yielding plates at the bases of rocking columns to dissipate energy.

Wada et al. [27] used a similar concept at the intermediate slender and tall columns. It was considered as a special column splice detail similar to the base yield plate connection to introduce rocking at a middle storey of slender truss-type-columns. The dynamic tests showed that the design was very effective in keeping the column compression under the design limit. Hence, this design concept was implemented in an industrial storage building in Japan.

A braced steel frame equipped with viscous dampers vertically between the column bases and the foundations was proposed by Tremblay et al. [28] as a cost-effective solution for enhanced seismic response of new and existing structures to severe earthquake ground motions. The numerical case study showed that the rocking response of the test frame could be predicted well using a simple finite element model that includes nonlinear viscous dampers and gap elements. It was shown from the results there was significant reduction in column uplift loads as compared to the traditional steel braced systems and confirmed similar case study structures could sustain design ground motion without structural collapse. The properties of the viscous dampers were verified though dynamic shake table testing. The test specimen for the shaking table test was a half-scale 2-storey braced frame where these viscous dampers were installed underneath the column base. Under a specific ground motion input of magnitude 7.0, there was a peak base rotation of 1.5%. The experiment confirmed the adequacy of the numerical models used to predict the response of such systems.

Sause et al. [29,30] studied an uplifting rocking frame system with PT strands that provide self-centring resistance. A similar study was undertaken by Eatherton et al. [19,31] with steel butterfly shaped fuses and BRBs were employed as replaceable energy dissipation devices. A shaking table test was conducted at Stanford-Illinois-TIT by Deierlein et al. [10,11]. The frame cost was more because of the dissipater, and the dissipater reduced the response. For both these studies, post-tensioned cables extend to the top of the structures. This post-tensioning method results in larger member sizes throughout the frame as compared to the case when post-tensioning is applied at the bases, but it obviates the need for the springs at the frame bases.

Sause et al. [30] proposed separating the rocking frame from the rest of the structure. Dissipaters between the frame and the rest of the structure may be placed to dissipate energy. Horizontal plates between the rocking frame and the structure behind may be used to transfer lateral forces, but not forces due to relative vertical deformation.

Wiebe [32] following Eatherton et al. [19,31] showed that providing multiple rocking sections over the height of a rocking frame system substantially reduced storey shears and bending moments due to system response of the first and higher modes. Including a non-linear, self-centring shear control brace at the first level of the frame can also be used to control the peak forces in the system [33-36]. Base rocking provides system deformation capacity, while the first-storey brace is only needed to limit the shears caused by the higher modes.

From around the time of the 2010-11 Canterbury earthquakes, structural steel has become the preferred construction material in NZ [8,9]. Steel frames, which are often concentrically braced, and may be easily connected using bolts or welds, are ideal for rocking structures. Several studies have been conducted on steel rocking systems and design guidance has been provided by Steel Construction NZ (SCNZ) [13].

SCNZ [13] state that in order to reliably predict the displacements of structures, that the ratio, β, of the lateral force resistance provided by dissipation devices (which yield in both tension and compression), V_{dev}, to that of the total yield strength, V_{total}, should be greater than 40% (i.e., β >0.4) but there is no upper-bound limit provided in the SCNZ guide on the amount of energy dissipation. This means that the lateral force resistance associated with gravity and post-tensioning force, V_{PT}, is less than 0.6 V_{total}, and $V_{dev}/V_{PT} > 2/3$. If V_{PT} is assumed to be bilinear elastic with zero post-elastic stiffness, the dissipater is assumed to be elastoplastic, and $\beta = V_{dev}/V_{total} = 0.40$ as shown in Figure 2, then the hysteresis loop is flag shaped and the lower force of the flag, V_{lower}, is $V_{PT} - V_{dev} = 0.6\ V_{total} - 0.4V_{total} = 0.2\ V_{total}$ (or $0.33V_{PT}$) as shown in Figure 2b. Because V_{lower} is positive, this means that there is no post-event residual displacement of the frame. Such a hysteresis loop which only passes through the zero displacement on displacement axis has been defined as "statically self-centring" [37]. For a structure with β > 50% (i.e., $V_{dev}/V_{PT} > 1$), then $V_{lower} < 0$ and upon unloading from the peak displacement there many significant displacements at zero force. Such loops do not possess static self-centring. Such a loop with a β ratio of 60% is illustrated in Figure 2c. In rocking frames without self-centring, manual re-straightening may be required and may be costly.

Dynamic self-centering is considered when a structure that does not possess static self-centering may still re-centre during a specific earthquake due to the interaction of dynamic damping and inertia forces, as well as potential contributions from the gravity system. Static self-centering is a more stringent requirement and will ensure that the rocking frame/wall fully re-seats after uplift and the structure returns to centre after all earthquakes.

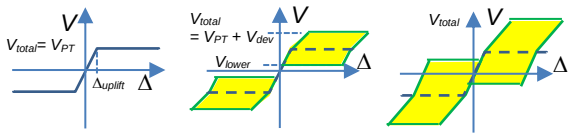

(a) PT alone ***(b)*** β = 0.40 ***(c)*** β = 0.60

Figure 2: Base shear (V) - roof displacement (Δ) response for elastoplastic structure with tension-compression dissipater.

Devices that carry both tension and compression force not only have the possibility of decreased static recentring, but during compression loading, they may also be susceptible to buckling and have difficulty with reseating. This may especially be a problem during earthquake bidirectional displacements as described by Gultom and Ma [38].

Tension Only Dissipation Device – GNG

There may be different ways to avoid the above problems in compression in rocking structures. One way to do this is to use tension only dissipation devices that only carries tensile force, and no compressive force. Types of tension only device include:

(i) A yielding tension cable carries force only in tension. However, force is carried only in the first tension quarter cycle to a specific tension displacement. In later shortening or elongation cycles to the same displacement, it carries no force.

(ii) A self-centring device which has tension resistance and energy dissipation in the tension-elongation force-displacement quadrant only through several cycles. A device with such a self-centring hysteresis loop, which can dissipate during many cycles, but which has limited peak displacement capacity while it is self-centring, and an increasing resistance with displacement, is described by Bagheri et al. [39], as well as others.

(iii) A ratchetting device, which dissipates energy in both the shortening and elongation tensile quadrants of the device hysteresis loop. Such a device is beneficial because the increased energy dissipation results in smaller peak displacements under shaking response cycles. In the rocking frame scenario, it is generally required to dissipate energy in the elongation tensile quadrant only (like the self-centring device described in (ii) above), however, it has the advantages that

   a. it can dissipate energy when there are both large peak and repeated cyclic displacements, and

   b. the dissipator inelastic force does not change with displacement, allowing smaller frame members foundations.

This ratchetting "tension only" dissipation device, also known as the "GripNGrab" (GNG) device, is used in the remainder of the paper. It consists of 2 parts – a ratchetting component (such as the behaviour of cable-ties), and a dissipation component which carries significant force only when the structure is yielding [23,40] as shown in Figure 3. Components have been built and tested [41-47] and analyses of rocking frames were conducted by Cook et al. [47] using tension-only devices, and by Rangwani et al. [16] using tension-only friction devices. They have also been used in yielding braced systems by Rad et al. [48].

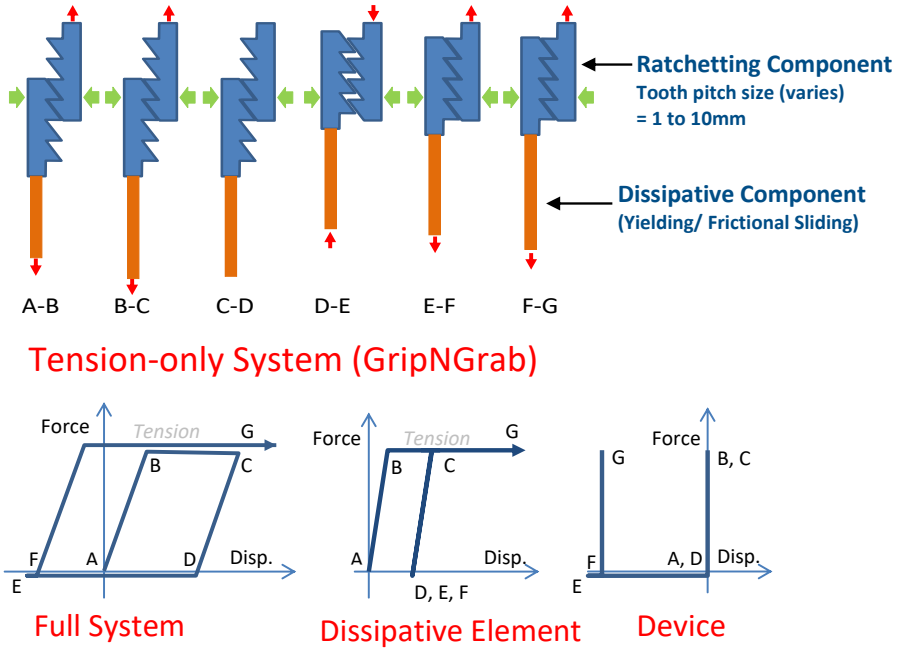

Figure 3: GNG device and behaviour [23,50].

When the device is engaged in tension, energy is dissipated via yielding/sliding in the yielding/frictional component. When the device is loaded in the compression direction, almost no force is carried, so it does not buckle but displacement occurs in the ratchetting component. This tension only direction of ratchet teeth engagement helps eliminate residual compressive forces as shown in Figure 3. The ratchetting during the shortening of the device as the frame/wall base returns to the foundation allows recentring. During tension loading, (wall uplift) there may be some free travel until the teeth engage during tension-loading. After the teeth have engaged, and the dissipater strength is reached, energy dissipation occurs. A detailed conceptual explanation of tension only device behaviour has been described in Figure 3. The device itself is shown with the teeth in blue. A small lateral compressive force is required to encourage the two parts not to remain in contact, so that the teeth engage. The dissipate element is shown in brown. Dissipation may occur due to yielding, frictional sliding or other means. Initially the device is loaded elastically in tension (A-B) then yielding/frictional sliding occurs in the dissipative element increasing its length (B-C). When the force is taken off (C-D) there is some elastic shortening of the dissipative element. When compression force is applied, the device carries very little compression but ratchetting occurs as the teeth in the ratchet slide relative to each other (D-E). This causes the compressive force to increase and decrease over this range, but it is not shown in the figure, because both levels of force are very small. The device maximum compressive axial force occurs when the teeth peaks on both side of the ratchet touch the peaks of the teeth on the other of the ratchet. This is when the maximum lateral expansion (and hence lateral compression) of the ratchet occurs. With further movement, the tooth peak on one side moves into the trough on the other side and the ratchet compressive force, and the device axial compressive force decreases. The peak ratchetting force is a function of the ratchet properties including tooth amplitude, friction within the ratchet, and the ratchet lateral compressive force holding the teeth on both sides together. This force should be small (say, 1% of the peak tensile force), so that buckling of the GNG system in compression does not occur. When tension force is applied again (E-F), the device undergoes free-travel until the teeth are engaged but the dissipative element does not change in length since the axial force in this stage is very small. The maximum possible free-travel distance in stage E-F is the tooth pitch. For greater tensions (F-G), displacement increases in the elastic range and then causes dissipation in the dissipative element as before [23,49].

To date, this ratcheting mechanism has been used only with yielding dissipaters eg: [41-47], but it can be used with any energy dissipation mechanism. Yielding dissipaters have a relatively low displacement capacity [48], but the GNG friction device can be made very long. In a rocking frame, the frictional GNG has a possibility of providing large displacements and full recentring, without undergoing significant damage. A preliminary study on the frictional GNG with a rocking frame was conducted by Livia and Yoo [51] where a small-scale experimental rocking model was used with frictional GNG to demonstrate this new concept. A rotational friction GNG is also being developed for testing on a brace in a 2-storey building in China where the dissipater ratchets in one direction and in the other direction the motion was controlled by the frictional bolts [52]. Due to rotational motion, it did not run out of stroke. However, this device may be costly.

There are two common means of dissipating energy using friction. These are the *symmetric friction connection* (SFC) and *asymmetric friction connection* (AFC) devices [53] SFCs, originally used by Pall & Marsh [54], Grigorian & Popov [55], provide the greatest sliding forces, so are discussed further here. A SFC consists of two thin high hardness shims [53] which sandwich a central steel element (such as a plate or section element) with slotted holes as shown in Figure 4**.** Additional external elements (plates or elements of a steel section) are placed either side, sandwiching the central slotted plate/element and shims. High strength structural bolts, with washers pass through the slotted hole and provide a clamping force so that friction can develop over sliding surfaces between the central plates and shims. Washers may be flat structural washers, or *conical spring washers* (CSWs), also known as *Belleville springs* (BeS).

When structural washers are used, bolts are generally proof loaded. When CSWs are used, there is the possibility of tensioning them to a lower fraction of the bolt proof load. Advantages of using such partially posttensioned CSWs (PPCSWs), as shown in Figure 4a, are that: the bolt will be unlikely to yield if, during sliding, the nut and bolt head are

forced apart; the compressive forces are spread out resulting in lower material degradation on the sliding surface; the sliding force can easily be adjusted by changing the bolt tension force; and repeatable performance may be obtained over many cycles [56,57]. However, high quality CSWs need to be designed and ordered from a limited number of suppliers, so they can cost significantly more than structural washers. Also, a longer connection, with more bolts and holes, may be required to obtain a specific sliding force as each bolt axial force is reduced.

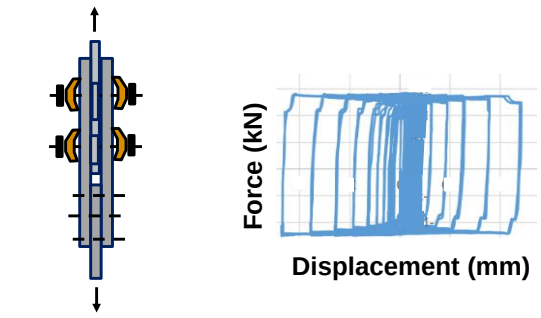

(a) SFC as friction sliding (tension) dissipater with CSWs [62]

(b) Hysteresis behaviour [61]

Figure 4: Sliding frictional component.

The SFC is so named because the resisting force on either side of the central plates are similar. Effective friction coefficients, μ_{eff} (defined as the sliding force divided by the number of bolts, number of surfaces, and bolt proof load) obtained from desirable hysteresis loops have been as high as 0.47 in connections with standard washers and proof-loaded bolts using Bisalloy 500 shims [58-60]. When CSWs have been used, desirable hysteresis loops have been demonstrated by Xie et al. [61] (as shown in Figure 4b).

For flat structural washers, with proof loaded bolts, the connection sliding force, f_s, may be obtained using Equation 1 [50,56] where n_{bolts} is the number of proof loaded bolts installed, n_{ei} is the number of effective interfaces (n_{ei} = 2 for a SFC), μ_{eff} is the effective coefficient of friction (obtained from experimental results), and N_{tf} is the bolt proof load. The equation can be obtained for PPCSW by using the actual axial force, N, instead of N_{tf}.

$$f_s = n_{bolts} * n_{ei} * \mu_{eff} * N_{tf} \quad (1)$$

It is possible to initially post-tension GNG tension-only devices. This may be easily conducted by connecting the device to the frame and leaving a gap below the base-plate connection immediately above the foundation. The bolts connecting this plate to the foundation may be tightened causing device tension and some frictional slip. Such post-tensioning was not considered in this particular study.

Displacement Prediction

It was seen in Figure 2, that for low device strengths, the energy dissipated may be small. SCNZ (2015) recommends $\beta > 0.40$ based on studies with tension-compression devices. based on studies with tension-compression devices. For tension-only devices, there is no compression resistance. Because of this, even if the SCNZ criteria is satisfied, the hysteretic energy dissipated during a full displacement cycle of a structure, with tension-only devices will be about one half of that for one using tension-compression devices with the same nominal yield force. This lower energy dissipation is likely to result in increased displacements. Furthermore, if lower dissipater strengths are used, then this may result in still greater displacements especially for structures expected to undergo many large displacement cycles, such as may be caused by long duration shaking from a long duration earthquake, or for a short period structure during a regular shaking event (e.g., Oscillation Resistance Concept (ORR) [63]). Displacements in the rocking frame systems are generally predicted using the methods below:

The equal displacement method assumes that structures with long fundamental period, T, will have the same peak displacements irrespective of the hysteretic dissipation characteristics [64]. Similarly, the equal energy method was also proposed and used widely used [3]. Berrill et al. [65] combined these concepts into one equation which gives the equal displacement concept for long period structures, and higher displacements for shorter period structures as a result of calibration of the relationship between lateral force reduction (R) (which is the same as k_μ in NZS1170.5 [66]) and ductility (μ). Vidic et al. [67], referencing Berrill et al. [65], propose a similar method. Variations on the Berrill et al. [65] method is now used in many standards worldwide (e.g. [66]). Various other methods of predicting the displacements of self-centering systems are discussed in papers by Seo [68], Rahgozar et al [69], Joo et al [70], and Zhang et al [71].

A substitute structure approach popularized by Gulkan and Sozen [72], for single storey structures, and used in ATC-40 [73] in the capacity spectra method, for multistorey structures, considers that the displacement response of an inelastically behaving oscillator may be found from that of an elastically responding oscillator with the same secant stiffness as the inelastically responding structure at the peak displacement and with a level of viscous damping which dissipates the same energy as the hysteretic energy dissipated. This concept, using an effective stiffness and effective damping, is also considered by Priestley et al [3]. However, it does not represent the behaviour of a range of hysteretic loops well, so the damping values were calibrated to enable the desired results to be obtained [74]. While the concept is simple, iteration is required to estimate the displacements. In many cases, similar results are obtained from this calibrated method to those from the calibrated R-T-μ approach, as would be expected.

Since the displacement response of structures may be greater than that from the NZS1170.5 [66] calibrated R-T-μ relationship, as a result of the low amount of hysteretic energy dissipated in a rocking frame, SCNZ [13] suggests that NZS1170.5 [66] displacements simply be multiplied by 1.3 [17] (Equation 2), Δ is the peak roof displacement, μ_{des} is the structural design ductility factor, and Δ_y is the yield displacement.

$$\Delta = 1.3\ \mu_{des}\ \Delta_y \quad (2)$$

Some issues with this approach are:

1 It predicts a displacement 1.3 times the elastic displacement, even when the shaking is small enough that the structure remains elastic. In such a case the structure is not rocking, so the 1.3 factor should not be needed. If it used only after rocking starts, the predicted response then has a discontinuity at the rocking point. FEMA356 [75], also with a displacement amplification for structures with pinched hysteresis loops, has similar issues.

2 It is not clear on how the period for use of this approach should be calculated, and damping values for calculation of the elastic displacement, which is used to compute μ_{des}, are also not provided. This means some assumptions are required so there is no unique SCNZ approach.

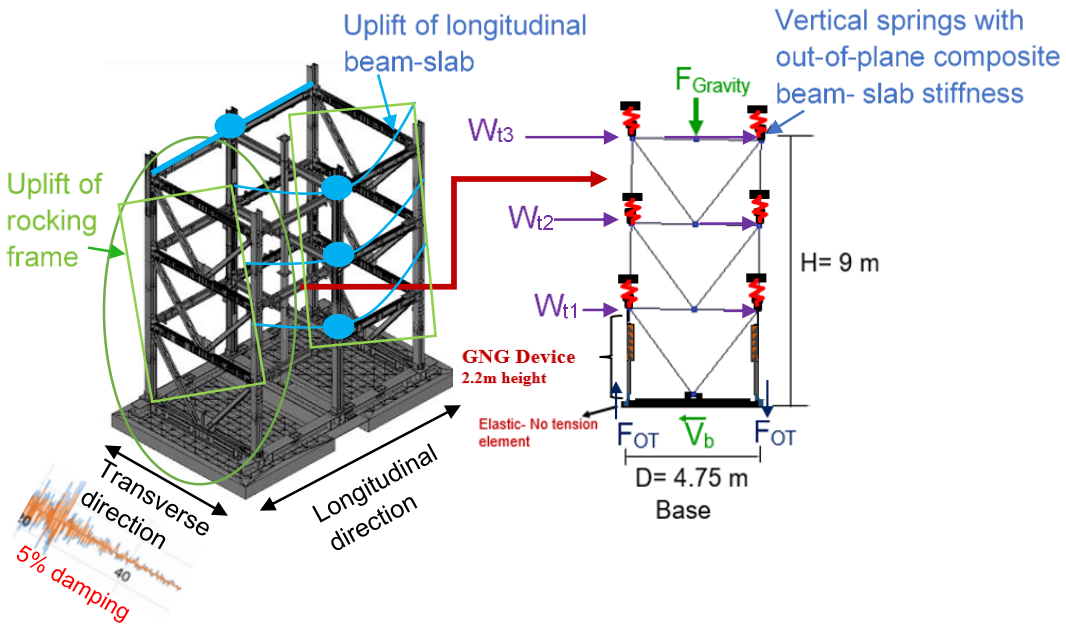

(a) ILEE Robust building *(b) Rocking frame model*

Figure 5: ROBUST rocking frame.

An improved approach proposed by Pennucci et al. [76] is shown in Equation 3. However, this method does not consider the effect of structural period, T, on the increase in structural response.

$$\Delta = R^{1.3}\,\Delta_y \tag{3}$$

METHODOLOGY

Rocking Frame Design Concept

The 9m tall 4.75m wide steel rocking frame with V braces was part of a building similar to the one used in ROBUST project [77,78] as shown in Figures 5a and 5b. The rocking frame is designed to be in Wellington (hazard factor, Z as 0.4) on soil class C with an importance level (IL) of 2. The near fault factor, $N\,(T, D)$ was taken as 1.0, as was the structural performance factor, S_p, and the serviceability factor, $R_s = 0.25$.

The rocking frame is in the transverse (short) direction. Frame gravity forces and seismic weight (W_t) were 117kN and 38.5 tonnes, respectively. The fundamental period was 0.16s based on the initial (pre-uplift) stiffness and seismic weight using eigenvalue analysis. This resulted in a seismic coefficient, $C_h(T) = 2.36$.

Design was conducted using the Equivalent Static Method (ESM) procedure (NZS1170.5 [66]). The reduced design level base shear and overturning moment (M_{OT}) demands were 90kN and 654kNm respectively using Equation 4 (NZS1170.5 Clause 5.2.1 [66]) where $k_\mu = R = \min\{1 + (\mu - 1)\,(T/0.7s),\ \mu\}$.

$$V_b = C_h(T) * R_s * Z * N(T, D) * S_p / k_\mu * W_t \tag{4}$$

The design requirements were [16]:

a) No uplift under wind loading (but no wind was considered here so this concept did not govern)

b) A lateral strength associated with a serviceability requirement ($\mu = 1$, $S_p = 1$, and $R_s = 0.25$) considering gravity and device overturning resistance, but not considering the beam-slab.

c) A lateral strength associated with a design ductility, $\mu = 3$, with $S_p = 0.70$ considering gravity, devices, and the beam-slab. It is noted that there is no limit on the actual ductility since slotted holes may be long providing significant inelastic displacement capacity.

The strength was controlled by the serviceability requirement. Also, the point of dissipater yield/sliding movement obtained when ignoring beam-slab resistance was chosen as the effective "yield point" to compute the period of the frame for design.

Specific Design Considerations

The required GNG strength contribution to the moment at the base of the structure, M_{GNG}, was obtained using Equation 5 according to the SCNZ rocking design guide [13], where M_{OT} is the base overturning moment demand, M_G is the moment resistance due to gravity force, M_{PT} is the moment resistance due to post-tensioning (PT), and M_{Slab} is the moment resistance from the longitudinal composite beam-slab that is uplifted by the rocking frame.

$$M_{GNG} \geq M_{OT} - M_G - M_{PT} - M_{Slab} \tag{5}$$

In the frame considered, gravity and “tension only” dissipater (i.e., GNG) forces, together with the longitudinal beam-slab effects, were sufficient to carry the design forces so posttensioning was not provided (i.e., $M_{PT} = 0$).

When the slab contribution is zero (i.e., $M_{Slab} = 0$), as is assumed to obtain the frame lateral design strength, the total moment resisted by gravity, M_G was 43% of the design overturning moment (M_{OT}). Therefore, the GNG resistance, M_{GNG} was $0.57M_{OT}$ which is greater than $0.4M_{OT}$ thereby satisfying the SCNZ [13] criteria.

A GNG device, with the ratchet and sliding symmetric friction connection (SFC) dissipater, providing this required strength is mounted at the base of the rocking frame as shown in Figure 5. Figure 6 illustrates the device itself. In the upper part, teeth in the rack plate engage with the those in the main body to provide the tension-only properties. High hardness shims are placed

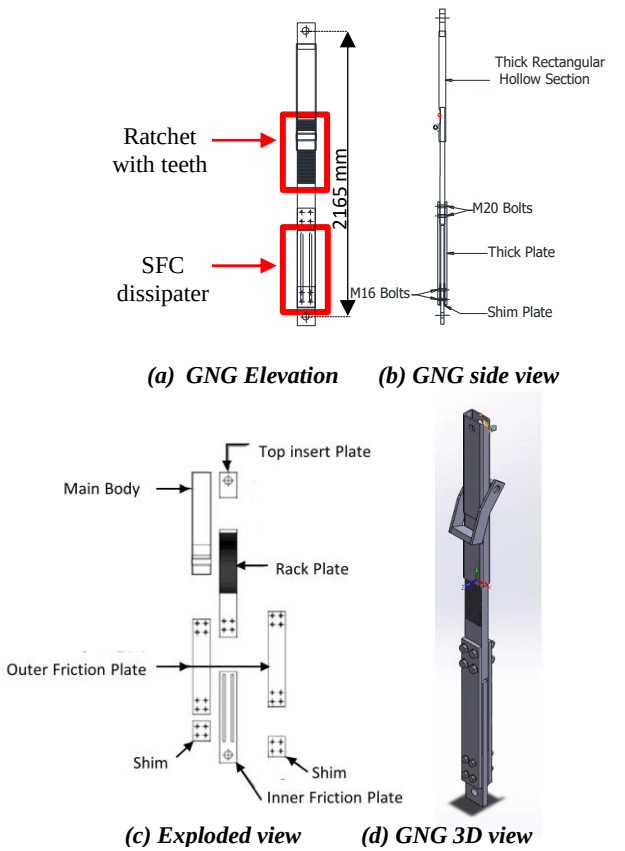

(a) GNG Elevation *(b) GNG side view*

(c) Exploded view *(d) GNG 3D view*

Figure 6: GNG device and components.

between the inner and outer plates where sliding occurs in the lower part of the device. More detailed information is available in [79].

The required GNG sliding strength of 80kN using one Grade 8.8 M16 bolt with 2 interfaces, using μ_{eff} = 0.47 and N_{tf} = 95kN the sliding strength, provided from Equation 1, was approximately 90kN. This considered the frictional dependable strength factor, ϕ, of 0.70. The minimum overstrength factor for design of the other frame components, ϕ_o, was 1.40 [23].

The steel frame and connections were designed to remain elastic during all levels of earthquake shaking. Inelasticity was possible only in the dissipator and due to flexural yield of the out-of-plane beam-slab resulting from frame uplift (as illustrated in Figure 1d). The steel frame design strength was provided according to MacRae et al [80]. This approach considers device overstrength, slab effects, and system inelasticity causing frame deformations to vary from that due to the lateral force distribution, and also the effects of other vertical columns in the structure. Such beam-slab deformation and yield may be avoided in frames where the rocking frame is separated (vertically de-coupled) from the gravity frames.

Modelling with GNG Device - Example Frame

The 2D steel rocking frame above was modelled in Open System for Earthquake Engineering Simulation (OpenSEES) [81], with a frictional GNG device. The device benchmark strength was 90kN for the inelastic analysis. It was also increased up to 200kN to understand the effect of this parameter on the response. This device strength range of 90 to 200kN corresponded to lateral force reduction factors, $R = k_\mu$, from 2.13 to 3.7 for the design level shaking. The value of 3.7 is slightly less than $1/R_s = 4$ considering the GNG strength provided, where R_s is the serviceability factor. The GNG hysteresis model developed by Cook et al. [46] was used. This model includes the tooth pitch and the free travel before the device takes up force as shown between E and F in Figure 3.

GNG Area Stiffness Selection and Verification

The GNG system stiffness depends on the component stiffnesses – the ratchet, the friction dissipater, and the connections (with the pawls, supporting arms, pins, bearings, and baseplate) [82]. As the dissipater extends due to frictional sliding in a tensile displacement excursion, the component stiffness can be expected to decrease slightly. If the GNG pre-yield axial stiffness is lower than considered during the design and modelling process, then structural drifts may increase. Also, sliding within the frictional dissipator may not occur for small uplift cycles if there is large elastic deflection within the GNG component. For the design conducted using available (realistic) properties of GNG parts and a design GNG force of 200kN to allow for significant overstrength, areas of the rack and rectangular hollow section shown in Figure 6 were 4896mm^2 and 1760mm^2 respectively. These values provided a maximum stress of 0.4f_y, where f_y is the yield stress of 300MPa. The lower of two areas, that is A_{GNG} =1760mm^2, was assumed to provide a reasonable approximation to the GNG system elastic stiffness at all extensions/lengths. Given the area of the dissipater, A_{GNG}, the steel elastic modulus E_s = 200GPa, the GNG length, L_{GNG} = 2.2m, and yield force, F_y, of 90kN, indicates an elastic deformation at yield, Δ_y, of about 0.54mm. To consider additional possible sources of flexibility due to the other GNG components and connections, a sensitivity analysis was carried out. The average GNG pre-yield axial stiffness, K_{GNG} obtained was 87272kN/m and 45545kN/m with respect to A_{GNG} of 1,000mm^2 and 500mm^2 respectively from Equation 6:

$$K_{GNG} = E_s A_{GNG}/L_{GNG} \quad (6)$$

A composite beam-slab section with a length of 3.625m in the frame out-of-plane direction also provided frame uplift resistance [77]. The beam-slabs are connected to the central transverse beam spanning between central columns in Figure 1. It is assumed that little uplift occurs at this location, thereby providing a fixed cantilever support, while uplift occurs at the beam ends where they are pinned at the rocking frame. In the OpenSEES model, this composite cantilever beam stiffness is represented by vertical springs shown in Figure 5b. These fixed node vertical springs were applied on each floor at each side of the rocking frame model (see Figure 5b).

The slab effective width is 536mm according to NZS3404 Clause 13.4.2.2 [83] and the beam column effective flexural stiffness was obtained using transformed area approach assuming full composite action. The vertical springs were assumed to have bilinear force-displacement properties with an effective stiffness of 3489kN/m and a strain hardening ratio, b as 0.0002. The composite beam-slab flexural strength, M_{y_slab} was 400kNm so the vertical force at the beam end causing this moment, F_{y_slab}, was 111kN.

Pushover (PO) Curve

The structure PO analysis curve is shown in Figure 7 up to a displacement of 100mm or 1.11% roof drift (taking the structural height as 9.0m), using the NZS1170.5 [66] lateral force distribution. P-delta effects did not significantly affect the response.

The **red** curve indicates the frame resistance provided only by gravity forces. The frame starts uplifting at 0.95mm roof displacement (0.0105% roof drift) at a base shear force, V_1, of 40kN.

The **green** curve, including the tension-only (GNG) device effects, indicates a lateral base shear strength, V_2, of 101kN. At

this point the peak roof and uplift displacements are 6.2mm (0.069% roof drift) and 2.0mm (0.042% θ_{base}), respectively. The device design tensile strength of 90kN was computed based on a 101 kN base shear force.

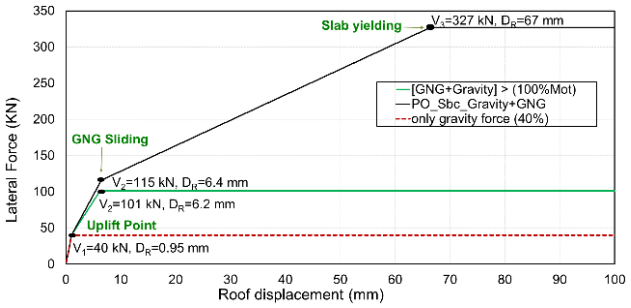

Figure 7: Pushover curve of 2D rocking frame GNG.

The **black** curve on the graph indicates the rocking frame resistance due to a combination of gravity, the GNG, plus longitudinal beam-slab effects. This curve reached a maximum of 327 kN at a peak displacement of 67 mm (0.74% roof drift). After this displacement, the beam-slab strength is reached.

This pushover analysis is consistent with earlier discussions where the ratio β of the base shear resulting from the device, V_{dev} (=61kN) to that of the total structure considering gravity loading and the device without the beam-slab, V_2 (=101kN), which is also V_{total} in our case, is 61%. The peak pushover displacement at peak strength was reached at 5.8 times the uplift displacement with gravity alone. The ratio, $\beta = V_{dev}/V_2$, is only 19% when the beam-slab effect is considered for the 500-year design level roof displacement following the SCNZ design guide procedure. The lower β is because of the higher V_2. Only the weaker frame without the beam-slab satisfies the SCNZ rocking frame design guide minimum limit, β, of 40%. The SCNZ recommendation was based on frames with tension-compression dissipaters as shown in Figure 2. For frames with tension only dissipators the energy dissipated is one-half of that for the same V_{dev}/V_2 considering the same peak displacement.

Building Torsional Considerations

As shown in Figure 5a, the rocking frame is part of a 3-D structure with the V-braced rocking frame and GNG device placed along the transverse direction as shown in Figure 5b. While only transverse direction shaking is considered, it is possible that irregularity in mass, stiffness, or strength, that building plan torsion could destabilize the structure. One step-by-step procedure to consider torsion, following the NZS1170.5 [66] approach, is explained below:

Step 1: Longitudinal frame base shear forces obtained due to torsion, $V_{frame,torsion}$ (Equation 7), assuming a mass eccentricity of 0.1*b*, where *b* is the building width, and *a* is the distance between longitudinal frames, are:

$$V_{frame,torsion} = V_b \times 0.1b/a = 90\text{ kN} \times (0.1 \times 7.25\text{m})/ 4.75\text{m} = 13.7\text{ kN} \quad (7)$$

Step 2: Longitudinal frame roof displacements due to torsion were found using frame analysis software with the NZS1170.5 [66] lateral force distribution to be 10.1mm, causing a plan twist, θ_{long}, of 10.06mm/(4.75m/2) = 0.004 rad. This in turn caused a rocking (transverse) frame roof displacement due to torsion of 0.004 rad x (7.5m/2) = 15.3mm. Since the transverse displacement without torsion under 2xDLS is 159mm, this gives a torsional component of 9.5% of the transverse displacement at this shaking level, but more at lower shaking levels.

Step 3: Beam end moments were 14kNm (from the torsional analysis) which is much less than the beam-slab nominal flexural strength, M_{y_slab}, of 400kNm the out-of-plane frames can easily stabilize the structure.

Column base moments due to torsion for corner (left and right) columns C1 and centre (along the longitudinal side) C2 column in the plan considered were 16.6kNm, 16.3kNm and 19.3kNm respectively. These were also significantly less than half their computed capacity indicating that any torsion, if it occurs, should not detrimentally affect the structure behaviour.

Frame Detailing

Representative GNG connections to the frame are shown in Figure 8. Shear rods, with nuts at the top allow uplift of the rocking frame columns to a specified frame rigid body rotation of 5% as shown in Figure 8a. Shear keys in Figure 8b resist horizontal base shear forces at the frame base brace intersection while permitting uplift. The GNG pinned base plate connection to the foundation is in Figure 8c. The horizontal view of GNG device is shown in Figure 8d.

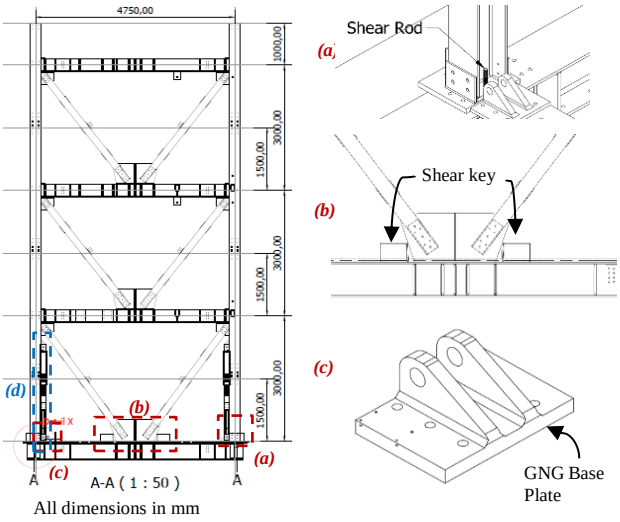

GNG Device connected pin-to-pin (horizontal view)

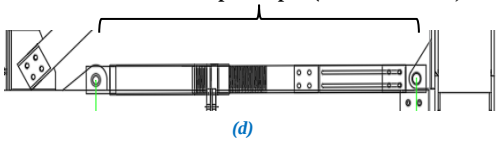

Figure 8: Rocking frame and component details.

Rocking Frame Displacement Prediction

The three approaches are considered for the prediction of rocking frame displacements without the beam-slab, as described in the literature section. They were (i) the SCNZ approach [13] based on the NZS1170.5 [66], (ii) the substitute structure method using information from [72-74] and (iii) a new approach introduced here.

The SCNZ approach estimates peak roof displacement (PRD), $\Delta_{roof,\ rocking}$, using Equation 8 which is based on Equation 2. The value of 1.5 approximates the "yield" roof displacement, $\Delta_{y,roof}$, divided by the "yield" centre of mass displacement, $\Delta_{y,CM}$, considering an inverted triangular lateral force distribution. These "yield" displacements occur after uplift occurs, and they are taken at the initiation of GNG sliding. The 1.3 is the magnification of displacement for rocking structures according to SCNZ [13] due to their pinched hysteresis loops. Also, μ_{des} is the design ductility found as a function of strength and period according to NZS1170.5 [66]. When the beam-slab effect is ignored, the "yield" base shear force-roof displacement point

(V_2, D_R=$\Delta_{y,roof}$) = (101kN, 6.2mm) according to the pushover curve in Figure 7.

$$\Delta_{roof,\,rocking} = 1.5 \times 1.3 \times \mu_{des} \times \Delta_{y,CM} \quad (8)$$

At the centre of mass, the displacement at GNG sliding, $\Delta_{y,CM}$, is 4.13mm so the secant stiffness to this point is 101kN/4.13mm = 24.5MN/m. Using the effective first mode mass, the period associated with this stiffness is 0.25s. Also, the damping is taken as 5% for a fully clad structure.

For the equivalent stiffness/damping approach from Gulkan and Sozen [72], the MDOF structure was transformed into an equivalent SDOF structure with an initial stiffness, mass and period obtained from Priestley [74]. Iteration was conducted to obtain the effective period was based on the secant stiffness, and the effective damping. This damping was obtained using the hysteretic energy dissipated in a full cycle of response to the peak displacement following Gulkan and Sozen [72] assuming an elastic stiffness corresponding to initiation of sliding. The Gulkan and Sozen [72] approach was used rather than the later calibrated versions because it is based on a fundamental concept. The roof yield displacement ($\Delta_{y,roof}$) was based on the GNG sliding point of 6.2mm as before.

Numerical Analysis

In addition to the nonlinear static pushover (NSP) analysis described above. Two other types of analysis were performed:

i) Nonlinear cyclic pushover (NCP) analysis of the 2D rocking frame model was performed using an inverted triangular lateral force pattern, and a small integration displacement increment between target displacements (often 0.00001mm). The peak target roof displacements, PTRD, used were the peak values obtained during nonlinear dynamic analysis (NDA) of the structure under the El Centro 1940 Array 9 NS record for the frame nonlinear dynamic analysis (NDA) conducted. The peak target roof displacements (PTRDs) in both the positive and negative directions from the NDA were considered. Before this, increasing PTRDs were used with different PTRD step sizes. For example, for DLS shaking for the frame with no beam-slab) the peak displacements from NDA were -75mm and +92mm. The PTRDs were to the following values (in mm): +0.5, 0, +1.0, -0.5, +1.5, -1.5, +2.5, -2.5, +3.5, -3.5, +4.5, -4.5, +5.5, -9.5, +10.5, -14.5, +15.5, -24.5, +25.5, -34.5, +35.5, -44.5, +45.5, -54.5, +55.5, -64.5, +65.5, -75, +92, +12.5 as shown in Figure 9.

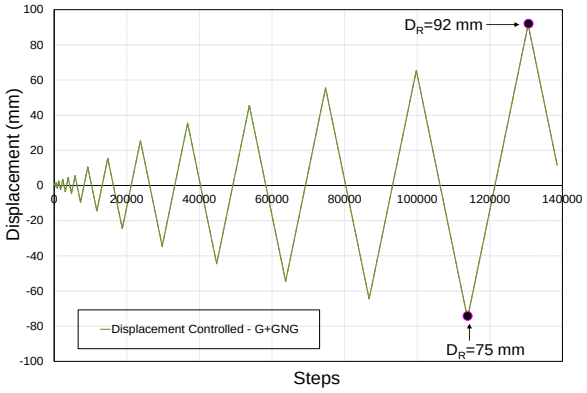

Figure 9: Roof PTRD history for frame with no slab.

ii) Nonlinear dynamic analysis, also known as inelastic dynamic time history analysis, was conducted using the Newmark β = ¼ method with an integration time-step of 0.01s and Newton-Raphson was used for convergence. The OpenSEES mass - tangent stiffness proportional Rayleigh damping ratio of 5% critical damping was applied in the first and 10th modes for the time history analysis [84]. Since the mass remained constant, this is simply tangent stiffness proportional Rayleigh damping. The ground motion (GM) record used for the TH analysis is IV El-Centro 1940 Array-9 with a recorded time-step as 0.005s. This record was selected because it matched the NZS1170.5 [66] spectral shape over a range of periods for ground type C. GM record response spectra was scaled for Wellington following the NZS1170.5 [66] procedure as shown in Figure 10. In addition, the record was scaled to different magnitudes. This is also known as incremental dynamic analysis (IDA).

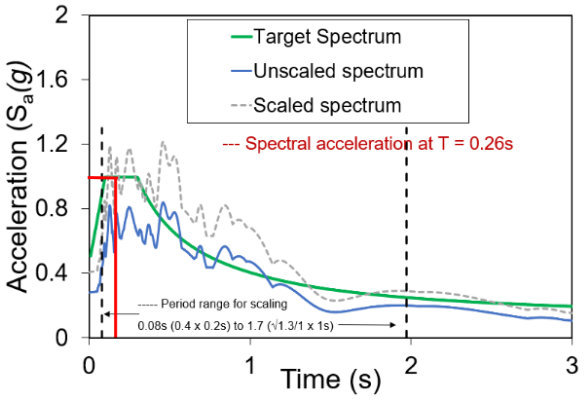

Figure 10: Response and target spectra from GM EC1940 Array-9.

The 2D linear and non-linear analysis of the rocking frame with the GNG device without and with slab effects were conducted. Parameters of interest were the absolute maximum peak roof lateral displacement (PRD), peak uplift displacement (PUD), cumulative uplift displacement (CUD), GNG forces and absolute maximum horizontal frame base shear forces. The PUD and CUD were measured beneath the centre of the column. The CUD was obtained during postprocessing using MATLAB. Geometric considerations are necessary to estimate the PUD and CUD at the location of the GNG device. The CUD at the GNG device, which is the sum of peak uplift values there, is important for friction dissipater length specification as it is a slight upper bound of the required dissipater inelastic displacement capacity due to tooth pitch and GNG stiffness effects.

BEHAVIOUR

Nonlinear Cyclic Pushover (NCP) Analysis

The deformation mechanisms at each step of pushover cyclic analysis without and with the beam-slab are shown in Figures 11 and 12, respectively. The backbone curves are consistent with the monotonic static pushover analysis of Figure 7.

In Figure 11, without the beam-slab effect, the symbol (a) indicates the frame in its at rest position. As the rocking frame is pushed laterally towards right lateral force resistance is provided by the gravity forces (i.e., Region A, Gravity Contribution). Uplift of the frame initiates at point (b) on the left side of the frame when the roof displacement is 0.95mm and the lateral resistance provided by gravity is overcome. As the frame is pushed further to a roof displacement of 6.2mm, the GNG dissipater attached to the base of the frame on the left side provides the lateral force resistance (i.e., Region B, Device Contribution). From this point (c), sliding of the left GNG dissipater occurs at a frame lateral shear force 101kN (i.e., Region C, sliding region) and the frame here rotates about the right base as a rigid body. After the PTRD at point (d) of 92mm is reached, corresponding to the PTRD from the NDA, elastic

unloading of the device occurs to point (e). From here until point (b), ratchetting of the GNG device occurs as the teeth within GNG device slide without force (i.e., Region D, ratchetting region) as described in Figure 3. Here, the GNG device is subject to very small compressive force, but because the force is very small, no buckling occurs. The whole unloading from (d) to (a) occurs without requiring any external force and guarantees recentering of the system if the frame itself remains elastic. When it has returned to (a), the structure is now not in its at-rest position, but it is likely to have significant velocity after the significant potential energy is released as it unloads from (d) to (a). As the frame deforms in the negative direction, it repeats the cycle above, but it has a reduced displacement (d') as a result of the record considered.

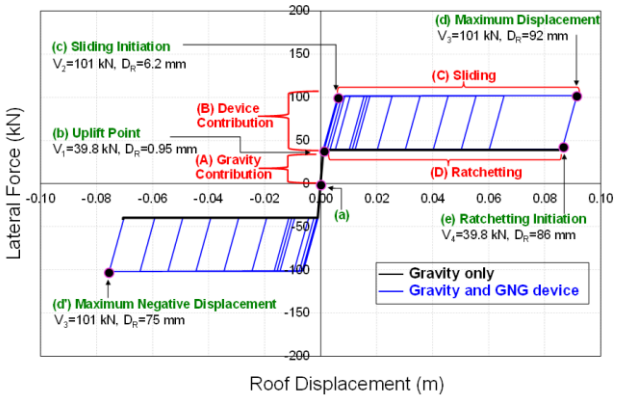

(i) Cyclic pushover curve.

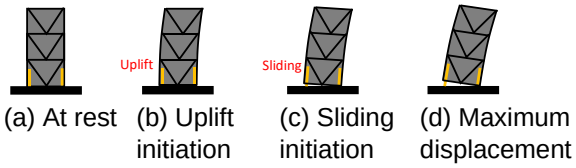

(ii) Frame monotonic deformations.

Figure 11: Deformation mechanisms at each step of cyclic pushover analysis at DLS level (with no longitudinal slab).

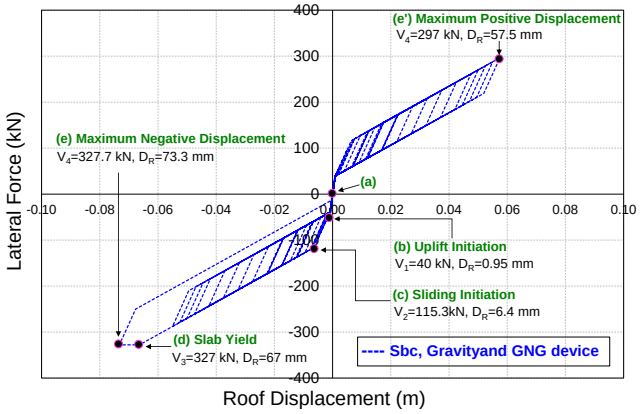

(i) Cyclic pushover curve.

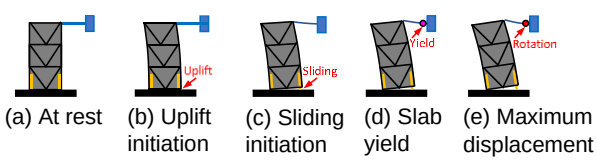

(ii) Frame deformations.

Figure 12: Deformation mechanisms at each step of cyclic pushover analysis at DLS level (with longitudinal slab).

For a frame (in the building transverse direction), the beam-slab acts in the frame out-of-plane direction (or building longitudinal direction) contributing to the frame lateral force resistance in addition to the gravity and dissipater effects as shown in Figure 12. Here, the label numbering is shown on the negative side of the graph because there is greater displacement in this direction. As in Figure 11, point (a) is at rest, and point (b) is uplift at a base a base shear, V_1, of 40kN. However, at point (c), V_2 increases from 101kN to 115kN as the beam-slab effect is also resisting the lateral force. The beam-slab effect also causes increased resistance as deformation further increases to (d) at 67mm (0.74% roof drift) where the slab starts yielding with a plastic hinge near the internal column. After this onset of slab-yielding the force remains the same at 327kN and does not further increase. The maximum displacement from the time history analysis of 73.3mm (0.81% roof drift) at (e) was used as the maximum negative PTRD. For the same record considered in Figure 12, the overall frame displacements were reduced by 20% and the beam-slab increased the lateral force resistance until it was 327.7kN/101kN = 3.24 times that of the Figure 11 frame.

Figures 13a shows the frame uplift behaviour at small drifts. The left base uplift occurs when the roof displacement moves to the right and vice-versa. Frame lateral force-roof drift, and force-uplift schematics are shown in the insert. In Stage 1, when lateral force is initially applied, the roof displacement increases, but the frame does not rock until a roof displacement of 0.95mm is reached at the uplift/roof displacement coordinate (D_U, D_R) of (0.0mm, 0.95mm). In Stage 2, both displacements increase until device sliding (2mm, 6.2mm) and the system remains elastic with no energy dissipation. Beyond this point (Stage 3), both D_U and D_R increase giving a different slope as energy dissipation device sliding occurs. This loading follows the lower curve in Figure 13a to the (D_U, D_R) points shown. Because rigid body displacement of the frame is occurring here,

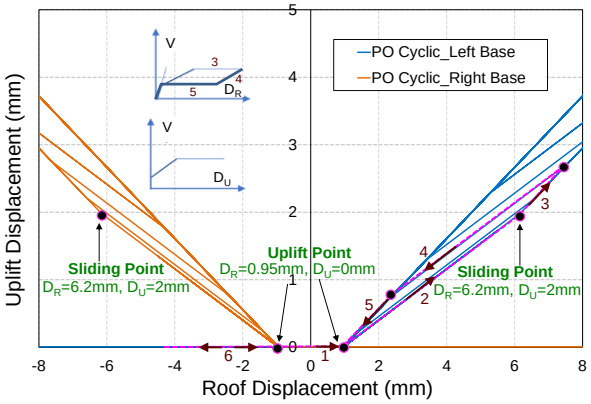

(a) Small displacement

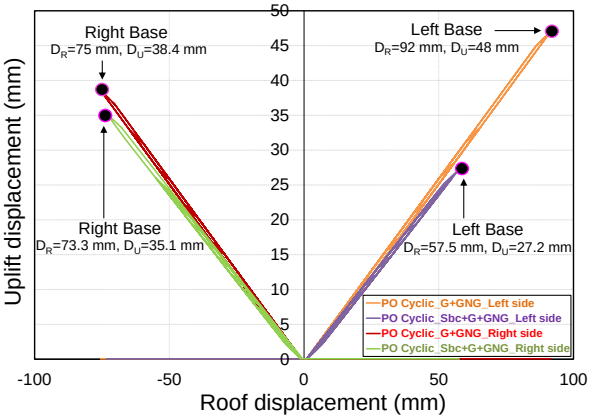

(b) Large displacements

Figure 13: Pushover cyclic uplift displacement vs roof displacement behaviour with and without longitudinal beam-slab at DLS displacements.

the ratio of D_U/D_R is equal to the frame base dimension divided by the frame height of 4.75m/9m = 0.527. On roof displacement reversal (Stage 4), the slope of the (D_U, D_R) curve is the same as that of Stage 2 (i.e., the elastic response from uplift until device sliding). This gives a line parallel to that in Stage 2. The next stage, Stage 5, occurs where there is ratchetting and the slope here is the same as Stage 3, and it continues until the base makes contact with the foundation (i.e., the uplift displacement becomes zero, $D_U = 0$). Thereafter, the roof elastic displacement decreases as the curve moves back toward, and past, the point (0mm, 0mm). No uplift occurs during this Stage 6 and the curve remains on the x-axis. Upon displacement reversal, there is no uplift again until point (b) in Figure 12, the uplift point (0.0mm, 0.95mm) is until a positive roof displacement is obtained. Until then the curve remains on the x axis (i.e., $D_U = 0$) in Stage 1. This is similar to the initial behaviour during Stage 1, except it does not necessarily start from the origin. The fact that the loading and unloading portions of the (D_U, D_R) curve are not on the same line, is due to the energy dissipation due to sliding with the SFC element. This small-displacement behaviour is the same for both the cases with and without slab effects and both curves are shown on top of each other here.

For greater drifts to the maximum PTRDs for both without the beam-slab effect and with the beam-slab Figure 13b gives D_U/D_R ratios at peak uplift of 48mm (left base) and 38.4mm (right base) respectively. The slightly lower ratio for the cases with the beam-slab is because the beam-slab is resisting the uplift, so the post-sliding behaviour is not purely rigid body rotation. Since these D_U/D_R ratios are similar and are slightly less than the rigid body value of 0.527, the rigid body approach gives a reasonable and slightly conservative estimate of the uplift behaviour at large displacements so it can conservatively be used for design.

Nonlinear Dynamic Analysis

Roof Displacements with and without Beam-Slab Effects

Figure 14 shows THA behaviour of the frames during the design level shaking (DLS) event described in the methodology on top of the cyclic PO behaviour without and with the longitudinal slab as shown in Figures 11 and 12.

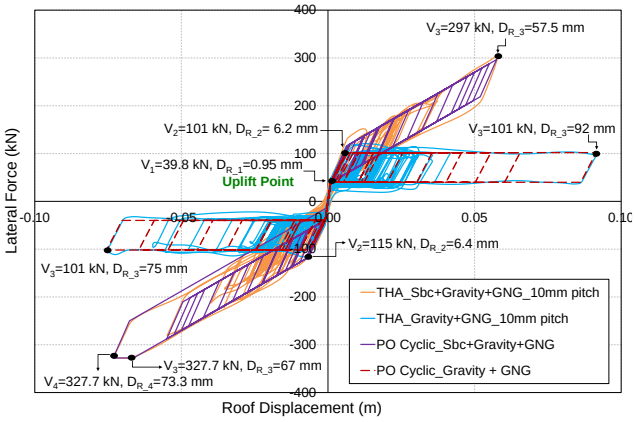

Figure 14: Comparison of pushover cyclic and THA at record DLS displacements.

The THA dynamic response indicates different forces than the PO curves because the instantaneous lateral force distributions change (i.e., they do not remain as the inverse triangular distribution) during the record, and this causes a variation in, including increased, base shear forces. If it is desired for the frame itself to remain elastic during this event, it should be designed for a base shear force associated with that from the THA. The increase is referred to as the base shear dynamic magnification factor in NZ standards. With the beam-slab, there is no increase for this particular record and shaking intensity. Specific response values are described using the Tables 1 to 4.

Detailed Response without Beam-Slab Effects

Table 1, showing roof, uplift, and cumulative, displacement demands, and corresponding lateral forces of the structure without longitudinal slab effects, indicate that GNG device sliding does not occur at a shaking intensity of 0.25xDLS because the GNG force, F_{GNG}, is less than the sliding strength of 90kN. As the shaking intensity, *MF*, is increased 4-fold from 0.5xDLS to 2xDLS, there is more a 10-fold increase in roof displacement, PRD, from 38mm (0.4% roof drift) to 366mm (4.07% roof drift). The PRD increase rate, being significantly greater than the *MF* increase rate, was attributed to (i) the short period of the structure, and (ii) the low hysteretic energy dissipation.

Over the same intensity range, left base uplift displacements increased from 13.3 mm (giving a base rotation, θ_{base}, of 13.3mm/4750mm = 0.28%) to 107mm (θ_{base} = 2.25%). The maximum peak uplift displacement, *PUD*, increased from 19mm (θ_{base} = 0.4%) to 192mm (θ_{base} = 4.04%) on the right base, and the maximum cumulative uplift displacements, CUDs, increased from 150mm to 1094mm at the same side of the structure. The effective number of peak uplift displacement cycles, N_{PUDc}, computed as the *max*{CUD} from both sides, divided by the *max*{PUD} from both sides considering each intensity level was 11.5 as shown in the Table 1. This is a useful design parameter for GNG ratchet and dissipater length and inelastic displacement capacity determination. Also, both the maximum N_{PUDc} and CUDs, do not occur at the same maximum or minimum intensity. It may be seen that the maximum device displacement of 1094mm is significantly larger than could be carried in a yielding dissipater, so sliding dissipaters with adjustable length may be more suitable for large displacements. An additional observation is that the maximum N_{PUDc} did not occur at the maximum or minimum shaking intensity level so care must be taken to ensure that an appropriate N_{PUDc} is used given the range and intensities which may occur. In all these cases residual/permanent displacements were zero for the model considered representing unimpeded re-seating.

The base shear at DLS was 120.7kN/101kN = 1.2 times that from the pushover strength. Further, that at 2xDLS was 144.8kN/120.7kN = 1.2 times than at the DLS, or 1.43 times the pushover strength and this needs to be considered in design if the 2xDLS intensity is to be considered. The reason for this increase is because the instantaneous lateral force distribution is different from and has a lower net centroid of force than the assumed lateral force distribution in the pushover analysis. Such effects have been considered before (e.g. [13, 74, 85-87]).

Detailed Response with Beam-Slab Effects

Table 2, where the slab effect is included, shows that for the same 4-fold increase in MF from 0.5xDLS to 2xDLS, PRDs increased 11.2-fold from 13.5mm (0.15% roof drift) to 159mm (1.76% roof drift). This is a similar increase to that when there was no out-of-plane beam-slab. The left base uplift displacements increased from 5.5mm (θ_{base} = 0.12%) to 51mm (θ_{base} = 1.07%) and right base uplift increased from 5mm (θ_{base} = 0.1%) to 81mm (θ_{base} = 1.7%). These roof and uplift displacement magnitudes were less than one half that in Table 1 where there were no slab effects. Lateral forces increased by approximately 3 times (i.e., from 120kN to 327kN at DLS) when slab effects were considered. This observation is consistent with Figure 14. For a shaking intensity of 0.25xDLS, the slab did not affect the behaviour because the structure did not uplift.

Table 1: Effect of shaking intensity (with no longitudinal slab).

Pitch 10 mm

MFx	$V_{b,max}$	**PRD**	**PRD**	**PUD**	θ_{base}	F_{GNG}	**CUD**	**RUD**	**PUD**	θ_{base}	F_{GNG}	**CUD**	**RUD**	N_{PUDc}	**RRD**
DLS	kN	mm	%	mm	%	kN	mm	mm	mm	%	kN	mm	mm		mm
				Left Base					Right Base						
0.25	65.9	3	0.04	0.6	0.01%	26.5	1.7	0	0.9	0.02	38.6	2.9	0	3.2	0
0.5	112.5	38	0.43	13	0.28%	90	148	0	19	0.40	90	150	0	8	0
1	120.7	92	1.02	47	0.99%	92	532	0	38	0.81	92	542	0	11.5	0
1.2	124.7	116	1.28	60	1.26%	92	575	0	44	0.93	92	512	0	10	0
1.4	129.5	136	1.51	71	1.49%	93	584	0	59	1.25	93	559	0	8	0
1.6	134.1	202	2.25	81	1.70%	94	805	0	106	2.22	94	780	0	7.6	0
1.8	138.2	294	3.27	91	1.93%	95	890	0	154	3.24	95	930	0	6	0
2	144.8	366	4.07	107	2.26%	95	1030	0	192	4.04	95	1094	0	6	0

Notation: MF = Shaking intensity magnification factor relative to DLS shaking, $V_{b,max}$ = Absolute peak base shear force, PRD = Absolute value of peak relative roof displacement, PUD = Peak uplift displacement, θ_{base} = base rotation, CUD = Cumulative uplift displacement, F_{GNG} = GNG force, N_{PUDc} = Effective Number of Peak Uplift Displacement Cycles = max{*CUD*}/max{*PUD*}, *RRD = Absolute value of residual roof drift, and RUD = Residual uplift displacement.*

Table 2: Effect of shaking intensity (with longitudinal slab).

Pitch 10 mm

MFx	$V_{b,max}$	**PRD**	**PRD**	**PUD**	θ_{base}	F_{GNG}	**CUD**	**RUD**	**PUD**	θ_{base}	F_{GNG}	**CUD**	**RUD**	N_{PUDc}	**RRD**
DLS	kN	mm	%	mm	%	kN	mm	mm	mm	%	kN	mm	mm		mm
				Left Base					**Right Base**						
0.25	69	3.1	0.03	0.6	0.01	23	1.7	0	0.9	0.02	36	2.9	0	3.2	0.0
0.5	140	13.5	0.15	5.5	0.12	90	75.6	0	5	0.10	90	76	0	15	0.0
1	328	73.3	0.81	28	0.58	91	502	0	35	0.74	91	607	0	17	-0.1
1.2	333	76.7	0.85	25	0.53	91	538	0	37	0.78	92	789	0	21	-0.2
1.4	338	85.5	0.95	26	0.55	91	468	0	42	0.88	94	1168	5	28	-8.8
1.6	346	103	1.14	32	0.66	91	320	0	51	1.07	95	1155	14	23	-26.0
1.8	354	139	1.54	39	0.81	92	607	1.4	70	1.47	96	1294	26	19	-46.4
2	357	159	1.76	51	1.07	94	1020	12.5	81	1.70	96	1059	22	13	-19.0

Notation: MF = Shaking intensity magnification factor relative to DLS shaking, $V_{b,max}$ = Absolute peak base shear force, PRD = Absolute value of peak relative roof displacement, PUD = Peak uplift displacement, θ_{base} = base rotation, CUD = Cumulative uplift displacement, F_{GNG} = GNG force, N_{PUDc} = Effective Number of Peak Uplift Displacement Cycles = max{*CUD*}/max{*PUD*}, *RRD = Absolute value of residual roof drift, and RUD = Residual uplift displacement.*

The PRDs obtained here were used as the PTRDs in the cyclic pushover analyses considering DLS excitation in Figures 11 and 13. These cyclic pushover uplift displacements of 48mm (or θ_{base} = 1.01%) (left base) and 38mm (or θ_{base} = 0.8%) (right base) with no beam-slab were the same as that from Table 1. This means that pushover analyses to DLS PTRDs provided an adequate estimate of PUDs, and that higher mode dynamic effects did not significantly alter these PUDs. Similar behaviour was observed for 2xDLS PTRDs.

Peak cumulative uplift displacements, CUDs, may be computed as N_{PUDc} x *PUD*, but appropriate N_{PUDc} must be used. As in Table 1, both the maximum N_{PUDc} and CUD, do not occur at the same maximum or minimum intensity. Further, they do not occur at the same intensity.

The base shear at DLS was 328kN/327.7kN = 1.0 times that from the pushover analysis at the same PRD of 73.3mm (or 0.81% roof drift). Similarly, the base shear at 2xDLS was 357kN/327.7kN = 1.09 times that from the pushover analysis, or from the DLS shaking, at the same PUD of 159mm (or θ_{base} = 3.35%).

Because beam-slab yielding occurs at a pushover roof displacement of more than 67mm and base shear of 327.7kN, the enclosed hysteretic area of the hysteretic loop is increased. Under 1.0 or more times the DLS shaking, residual roof displacement, RRD, and residual uplift displacement, RUD, occur. Figure 14 indicates from the cyclic pushover analysis that there should be no RRD at 1xDLS shaking, bit it occurs because dynamic effects change the lateral force pattern from the assumed code distribution. The RUD is greater on the side of the structure with greater PUDs. It is noted that the residual displacement is caused by slab yielding, rather than by any GNG effect. For large RRD up to *MF* of 1.6, the RUD on at least one side of the structure is zero, so the frame rotates like a rigid body and RUD/RRD is approximately 4.75m/9m =0.53. For *MF* of 1.8 and 2.0, |RRD| is approximately $|RUD_{left} - RUD_{right}|/0.53$ again indicating rigid body rotation. However, the fact that RUD exists on both sides of the frame, it indicates that the whole frame has uplifted, and it is suspended from the yielding slab. This situation is not desirable. These issues with permanent roof and uplift displacements, may be avoided if such systems are designed so that the beam-slab does not yield.

Overall, the effect of providing the beam-slab, as shown by comparing Tables 1 and 2, it may be seen that:

- The frame base shear strength with the beam-slab was up to 3.2 times greater than without the beam-slab, indicating greater required member and foundation sizes to resist these forces
- Peak roof displacement with the beam-slab was as low as 43% of that compared to the frame without the beam-slab, indicating less severe demands on the building non-skeletal elements.

- PRDs increased by around 10 times in both cases when changing the shaking magnitude from 0.5xDLS to 2xDLS. This large increase is likely due to the short period of the structure and low energy dissipation.
- Peak uplift displacement (PUD) could generally be slightly conservatively estimated using a rigid body rotation assumption for the frame in both cases.
- Cumulative uplift displacements, CUDs, needed to determine the GNG length and inelastic displacement capacity were of the same order of magnitude both with and without the beam-slab effect.
- The equivalent effective number of peak uplift displacement cycles (N_{PUDc}) were up to 28 with the beam-slab, rather than 12 without it. These did not occur at the maximum shaking intensity.
- With the beam-slab, yielding occurred there. Under high levels of shaking this resulted in undesirable permanent displacements and in total uplift of the rocking frame. There were always no residual displacements when no beam-slab was considered.

Sensitivity of GNG to Tooth Pitch

Tables 3 and 4 show that the effect of tooth pitches from 1mm to 10mm (the value used earlier), during shaking to the DLS level. Greater tooth pitch causes greater slackness within the hysteresis loop. It may be seen that:

i) when no slab was considered, the PRD was about 92mm, and the PUD increased from 43mm to 47mm for the left base and varied between 35mm and 42mm for the right base. This is also shown in Figure 15.

ii) when slab effects were considered, PRD increased from 28mm to 73mm, and PUD increased from 9mm to 28mm for the left base and from 12mm to 35mm for the right base as shown Figure 16.

The tooth pitch effect was more significant on the structure with slab effects, possibly because N_{PUDc} was greater.

At 2xDLS, the increase in tooth pitch for frames without and with slab effects did not significantly affect PRDs and PUDs as shown in Tables 3 and 4; also, the displacement lines overlapped as shown in Figures 17 and 18. In fact, a smaller pitch of 1mm resulted in increased PUD on left base from 107mm to 123mm as compared to with greater tooth pitches when there was no slab.

An increase in tooth pitch from 1 to 10mm increased the CUD of the left and right base approximately 2.1 and 1.4 times at DLS and 2xDLS, respectively where there was no slab. Also, where the slab effects were considered, an increase in tooth pitch from 1 to 10mm increased the CUD of the left base approximately 3.1 and 1.3 times and right base approximately 3.2 and 0.89 times at DLS and 2xDLS, respectively.

The residual frame and uplift displacements (RRD and RUD) were zero when there was no beam-slab at both shaking levels. At the DLS level, even with a beam-slab there was no residual displacement, but when the shaking level increased, the beam-slab yielded and the RRD increased to 29.2mm (0.32% roof drift) and RUD to 23mm (0.48% θ_{base}).

Table 3: Effect of tooth pitch (with no longitudinal slab).

MFx	**PS**	$V_{b,max}$	**PRD**	**PRD**	F_{GNG}	**PUD**	θ_{base}	**CUD**	**RUD**	**PUD**	θ_{base}	**CUD**	**RUD**	N_{PUDc}	**RRD**
DLS	mm	kN	mm	%	kN	mm	%	mm	mm	mm	%	mm	mm		mm
						Left Base				**Right Base**					
1	1	121	85	0.94	91	43	0.91	240	0	38	0.80	255	0	6	0
	3	121	81	0.90	92	41	0.86	278	0	35	0.73	314	0	7.7	0
	5	121	91	1.01	92	47	0.98	379	0	41	0.87	373	0	8	0
	10	121	92	1.02	92	47	0.99	532	0	38	0.81	542	0	11.5	0
2	1	145	366	4.06	95	123	2.59	717	0	192	4.04	781	0	4	0
	3	145	366	4.07	95	107	2.26	765	0	192	4.0	798	0	4	0
	5	145	366	4.07	95	107	2.26	739	0	192	4.04	823	0	4	0
	10	145	366	4.07	95	107	2.26	1030	0	192	4.04	1094	0	6	0

Note: PS- Pitch Size, other notations in Table 1.

Table 4: Effect of tooth pitch (with longitudinal slab).

MFx	**PS**	$V_{b,max}$	**PRD**	**PRD**	F_{GNG}	**PUD**	θ_{base}	**CUD**	**RUD**	**PUD**	θ_{base}	**CUD**	**RUD**	N_{PUDc}	**RRD**
DLS	mm	kN	mm	%	kN	mm	%	mm	mm	mm	%	mm	mm		mm
						Left Base				**Right Base**					
1	1	192	28	0.31	90.5	9	0.18	161	0	12	0.26	192	0	16	0
	3	240	40	0.45	90.6	16	0.35	282	0	19	0.40	293	0	15	0
	5	208	32	0.35	90.5	12	0.25	272	0	14	0.30	291	0	21	0
	10	328	73	0.82	90.7	28	0.58	501	0	35	0.74	607	0	17	0
2	1	356	156	1.73	95	48	1.01	789	6.5	79	1.67	1184	22	15	28.4
	3	359	152	1.69	95	49	1.04	817	7.6	77	1.62	1063	23	14	29.2
	5	355	153	1.70	94	48	1.01	859	8.2	82	1.72	989	23	12	28.1
	10	357	159	1.76	94	51	1.07	1020	12.5	81	1.70	1059	22	13	19

Note: PS- Pitch Size

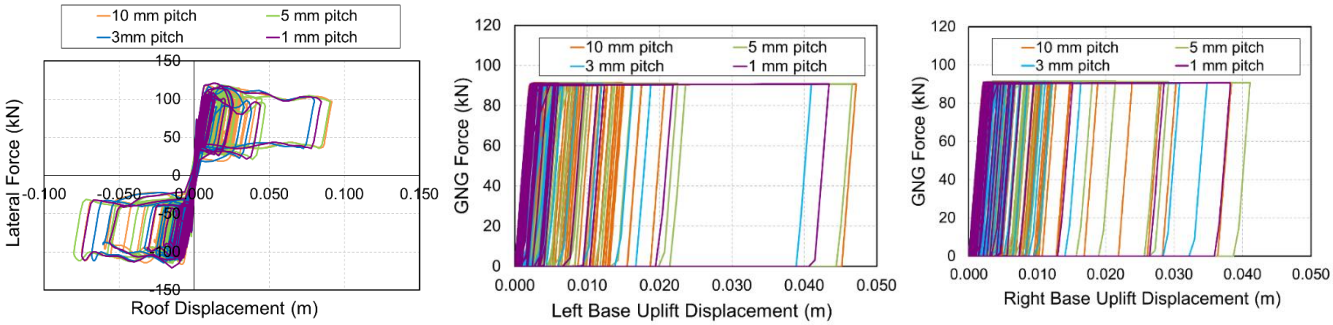

(a) *(b)* *(c)*

Figure 15: Effect of tooth pitch - DLS shaking (without longitudinal slab).

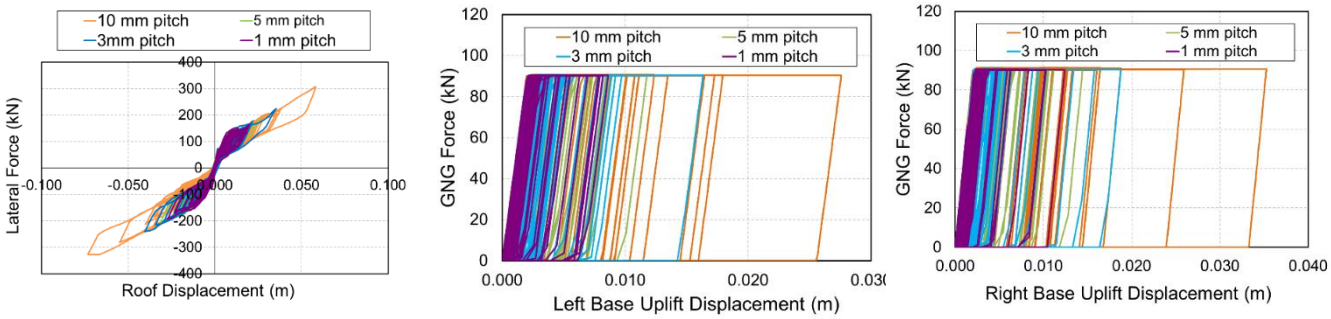

(a) *(b)* *(c)*

Figure 16: Effect of tooth pitch - DLS shaking (with longitudinal slab).

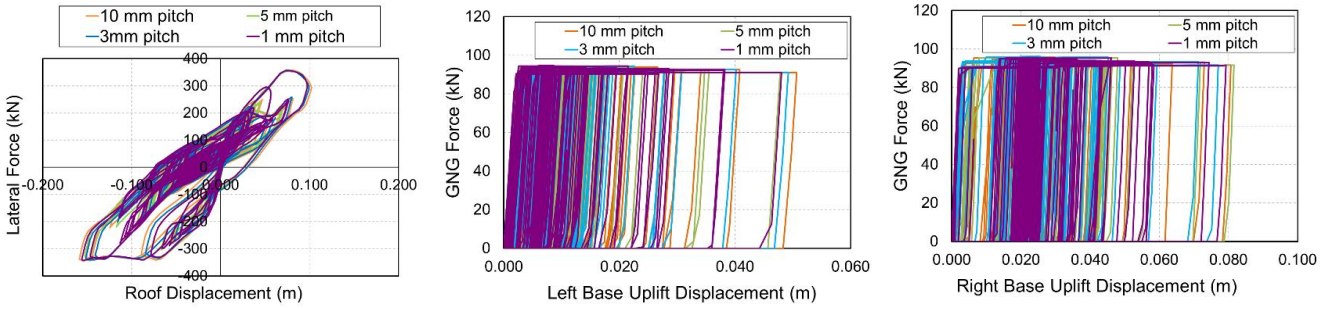

(a) *(b)* *(c)*

Figure 17: Effect of tooth pitch – 2xDLS shaking (with longitudinal slab).

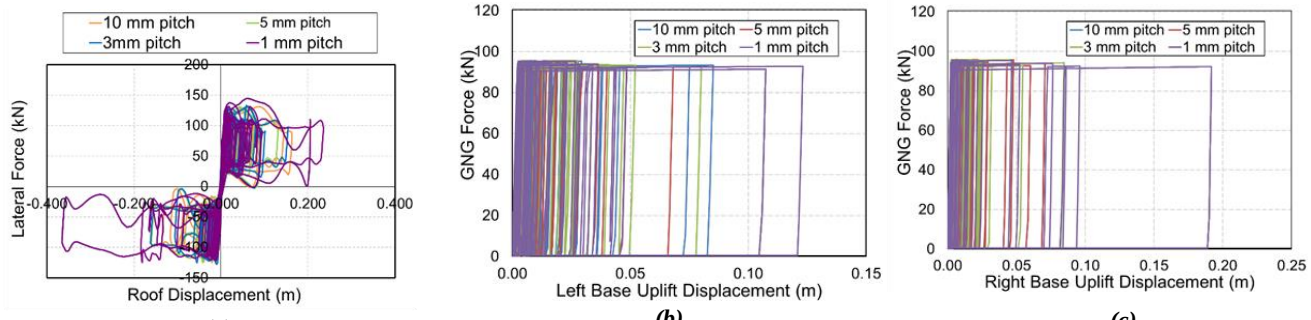

(a) *(b)* *(c)*

Figure 18: Effect of tooth pitch – 2xDLS shaking (without longitudinal slab).

Sensitivity to GNG (Pre-Yield) Axial Stiffness

Figure 19, using a GNG strength of 90kN, indicates that the lateral force-roof displacement curve was relatively insensitive to different GNG area (and pre-yield axial stiffness) values over the practical range considered.

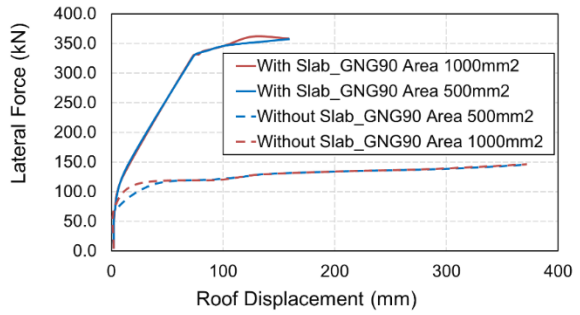

Figure 19: Effect of GNG area/stiffness on lateral force vs roof displacement for frame with and without longitudinal slab effect using Incremental Dynamic analysis (IDA) with 0 to 2 times DLS for the El Centro 1940 NS motion, ζ = 5%.

Displacement Considerations

Table 1, shows that the frame peak roof displacement (PRD), ignoring beam-slab stiffness effects, from time history analysis under the DLS intensity was 92mm (1.02% roof drift). This is also shown in Figure 20 as well as for other shaking intensities. This 92mm is much greater than the NZS1170.5 [66] DLS response spectrum of 15.5mm for the period of 0.25s.

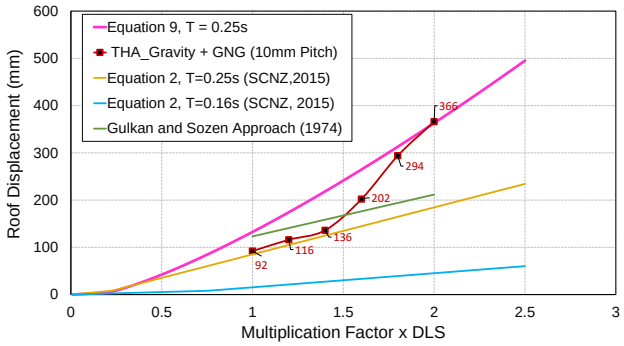

Figure 20: Predicted and actual peak roof displacement vs multiplication factor (MF) x DLS.

The increase of the DLS PRD above the spectral displacement level are due to the following reasons which standard prediction methods consider, and which have been discussed earlier:

(i) the roof displacement being greater than that at the CM,

(ii) the short period structure having greater inelastic ductilities than longer period structures for the same lateral force reduction factor (k_μ), and

(iii) the shape of the hysteresis loop.

As a result, DLS PRD predictions from the NZS1170.5 [66], SCNZ [13] methods of 65.4mm and 85.0mm were obtained. These are also less than the value of 92mm obtained.

Differences for the low predictions from these methods to predict PRD for an inelastically responding multistorey structure may be due to:

a) The definition of initial period used in the displacement prediction. It was based on the secant stiffness to the point of device sliding initiation, rather than first uplift.

b) The base shear strength and roof lateral "yield" displacement associated being based on the lateral force distribution assuming a first mode response, and no reduction in base shear due to multiple mode effects.

c) The nominal strength of the GNG device used the dependable value, ϕ, of 0.70. This was considered in design, causing k_μ < 4 so the structure analysed was stronger than that considering the k_μ = 4 expected due to the use of R_s = 0.25. The effective lateral force reduction factor, k_μ, for the NZS1170.5 [66] DLS shaking is computed as the NZS1170.5 [66] DLS elastic spectral displacement (which occurs at the centre of mass, CM) of 15.5mm, divided $\Delta_{y,CM}$, of 4.13mm. That is k_μ = 3.74.

d) The inaccuracy of the empirical methods of NZS1170.5 [66] and SCNZ [13] to predict displacements (i.e., the k_μ-*R* relationship), and

e) For the analysis record, the spectral displacement at *T* = 0.25s was 18.2mm. Therefore, the shaking intensity was ((18.2mm/15.5mm - 1) x 100% =) 18% greater than from NZS1170.5 [66]). This means that k_μ = 1.18 x 3.74 = 4.41.

For k_μ = 4.41, μ_{des} is 10.55 according to Clause 5.2.1.1 in NZS1170.5 [66]. The SCNZ [13] prediction of $\Delta_{roof,\ rocking}$ (i.e., PRD) is 1.5 x 1.3 x 10.55 x 4.13mm = 85.0mm according to Equation 8, and the NZS1170.5 [66] prediction is 1.5 x 10.55 x 4.13mm = 65.4mm as stated earlier.

Similarly, for a shaking corresponding to twice this intensity (i.e., 2xDLS or *MF* = 2), k_μ = 2 x 4.41 = 8.82, and μ_{des} is 22.90, and $\Delta_{roof,\ rocking}$ (i.e., PRD) is 184.56mm (2.051%) according to the SCNZ [13] prediction from Equation 8. The NZS1170.5 [66] prediction was 142.0mm. The NZS1170.5 [66] requirement considering the limit of T of 0.4s for design was not used as we are using the actual record. The predictions were both less than that from the analysis of 366mm as shown in Table 1.

Gulkan and Sozen's simple single degree of freedom equivalent period-damping method [72], which involved iteration, gave DLS PRD and ductility predictions of 123.2mm (1.37% roof drift) and 20.4 respectively. Similarly, under 2xDLS, the predicted ductility demand is 34.9 and the displacement is 212mm (2.35% roof drift). These PRD predictions are 1.34 times that obtained for the DLS intensity of 92mm (1.02% roof drift), but it is only 58% of the 366mm (4.07% roof drift) obtained at 2xDLS.

The DLS maximum of the peak uplift displacements of the structure without the beam-slab from both sizes of the frame, PUDs, predicted from the NZS1170.5 [66], SCNZ [13], and equivalent stiffness-damping [72] methods were 30.7mm, 40.8mm and 61.8mm respectively as (*PRD*-$\Delta_{y,roof}$) x 4.75m/9m, using $\Delta_{y,roof}$= 6.2mm (0.069%). The THA PUD is 47mm (Table 1).

Figure 20 shows that the SCNZ method slightly underpredicts the time history peak roof displacement response (maroon curve) when the shaking intensity is less than about 1.4xDLS (i.e., *MF* < 1.4) considering (*T* = 0.25s (brown line). For greater *MF*, the PRD increases rapidly, and it becomes approximately twice the SCNZ prediction at *MF* = 2. For the SCNZ prediction considering the initial elastic period associated with 0.16s (i.e., no uplift) as shown by the blue line, the prediction is significantly lower.

The equivalent stiffness-damping method [72] (as shown in the **green** line) estimates larger displacements (roughly 1.1 to 1.4 times) than that from the SCNZ method (with *T* = 0.25s). These results obtained from equivalent stiffness-damping method are conservative for shaking intensities, *MF* < 1.6. The time history response became 1.73 times the prediction at *MF* = 2.

From the discussion above, it is clear that the displacement prediction approaches do not match TH analysis results for the cases considered. Thus, a new approach is considered to overcome the inadequacies of the existing approach. Equation 9 [24] provided an empirical prediction equation for this case, where μ_{des} is the structural ductility obtained using standard code methods (e.g., NZS1170.5 [66]), α is a power factor. and Δ_e is the elastic displacement. The second term in the bracket controls when $\mu < 1$, for elastic structures.

$$\Delta_{CM} = \max \{\mu_{des}^{\alpha} \Delta_{y\_CM}, \Delta_e\} \quad (9)$$

This method has the following advantages:

(i) immediately before and after the sliding (or uplift) displacement is reached, there is no step function in the displacement as there is in the SCNZ method,

(ii) it considers the short period increase in displacement above the elastic level, making it superior to the method by Pennucci et al [76].

(iii) it can be tailored to represent the actual response.

In this study, for this particular structure, α is 1.3 as shown by pink line on Figure 20. For the structure with a slab effect, the value of α was 1.03. While this approach shows some promise, full calibration considering hysteresis loop shape, lateral force reduction factor, period, and a range of records is required.

The sensitivity of the TH analysis to earthquake magnitude shown in Tables 1 and 2 are a result of the structure being short period (and therefore subject to many displacement cycles), and also to the pinched nature of the hysteresis loop (with its low energy dissipation), according to the Oscillation Resistance Concept (ORR) [63, 77].

CONCLUSIONS

A rocking frame with GNG tension-only devices at the base columns is studied using pushover, and time history analysis considering different intensities. The effect of the out-of-plane beam-slab on response was also evaluated. It was found that:

1. A rocking frame system with frictional tension only energy dissipaters was developed. The tension only device provides no resistance to frame recentring, and the frictional dissipater allows large displacements and easy reinstatement after a large shaking event. The design of the 3-D frame included a simple method to consider torsion and some details for attachment of the device to the frame were described.
2. Under cyclic pushover analysis, the deformation mechanism was easily understood, with and without beam-slab contribution. It was shown that the required length of frictional dissipater (and consequently the inelastic displacement capacity) increased with greater cycles. For the frame without beam-slab effects, the lateral strength resulting from the dissipater, divided by the total frame lateral strength was 61%. This value satisfied the SCNZ minimum requirement of 40%, but with half of the energy dissipation. With the slab, the frame was stronger, and the ratio was 19%. The rigid body rocking behaviour gave good, but slightly conservative estimates of the peak uplift displacements from the peak roof displacements.
3. For the frame without beam-slab resistance to lateral displacement, the peak response for this short period structure with a low amount of energy dissipation was several times higher than the elastic response. As the shaking intensity increased from the design level shaking (DLS) to 2xDLS, the frame roof displacements increased by 4 times for this short period structure, uplift displacements for left and right base increased by 2.3 times and 5 times respectively, cumulative uplift displacements (CUDs) for left and right base increased by 1.94 times and 2 times, and there were no permanent displacements indicating unimpeded re-seating. The cumulative uplift displacements, which are necessary to determine the tension-only device inelastic displacement capacity, were 11.5 and 6.0 times the peak uplift displacement under shaking levels corresponding to DLS and 2xDLS levels respectively. The maximum frame base shear force demand was up to 1.43 times the maximum base shear from cyclic pushover analysis due to the lateral force distribution differing from that assumed.
4. When the effect of the beam-slab was considered, as the shaking level increased from the design level shaking (DLS) to 2xDLS, the frame roof displacements increased by 2.2 times, uplift displacements for left and right base increased by 1.82 and 2.3 times respectively, cumulative uplift displacements (CUDs) for left and right base were 2 and 1.74 times respectively the peak uplift displacements. The cumulative uplift displacements (CUD) were 17 and 13 times the peak uplift displacement (PUD) under shaking levels corresponding to DLS and 2xDLS levels respectively. The maximum ratio of CUD to PUD of 28 occurred at an intermediate shaking intensity of 1.4xDLS. Beam-slab yielding occurred as a result of significant uplift at large roof displacements during large shaking intensity events resulting in permanent roof and uplift displacements. The maximum frame base shear force demand in the time history analysis was up to 1.09 times the maximum base shear from cyclic pushover analysis with the code lateral force distribution.
5. The frame performance with the beam-slab compared to that without the beam-slab in the case studied was different in the following ways: (a) the base shear increased by 3.2 times (indicating greater required member and foundation sizes), (b) peak roof displacements reduced to as low as 43% (indicating less severe demands on the building non-skeletal elements), (c) permanent displacements were possible (requiring post-event repair), and (d) there were up to 2.3 times more excursions to the peak uplift displacement. The increase in peak roof displacement and cumulative uplift displacement with shaking intensity, were similar in both cases.
6. For the range of parameters investigated, the effect of GNG strength on roof displacements was not significant but increasing GNG strength increased the base shear. The response was also not generally sensitive to GNG tooth pitch except during small magnitude shaking with beam-slab effects considered. The response was not sensitive to GNG stiffness.
7. Peak roof displacement (PRD) prediction using the SCNZ method assumed a certain amount of energy dissipation. Only one half of this was provided with the tension-only devices indicating a modified prediction method was required. For the cases considered, the PRDs at DLS for the current frame were almost twice those predicted by standard methods (e.g., SCNZ and an equivalent-stiffness/damping approach) where the yield point was defined at the initiation of device sliding. A simple improvement to the *R-T-*μ relationship was developed to match the observed behaviour for the model building considered when subjected to a large range of shaking intensity.

ACKNOWLEDGEMENTS

This work described is part of a joint NZ-China research programme with the International Laboratories on Earthquake Engineering (ILEE), Tongji University, Shanghai, China and directly with Tongji University, Shanghai, China. Direct NZ funding is kindly provided by the Building Research Association of NZ (BRANZ) under the Building Research Levy, the Earthquake Commission (EQC), the HERA Foundation (a charitable trust associated with HERA), QuakeCentre, the Tertiary Education Commission funded QuakeCoRE (the NZ ILEE partner through whom the NZ funding is also coordinated), and the University of Auckland (UA). Donations of materials is kindly provided by Comflor, Hilti Corporation, TrackLok, Gripple, Lanyon & LeCompte Construction Ltd., and Alutech Doors & Windows Ltd and Catalyst company. Expertise has been generously provided by a number of NZ industry representatives. The authors gratefully acknowledge this support. Opinions expressed are those of the authors alone. The QuakeCoRE paper number is 0711.

REFERENCES

1 Housner GW (1963). "The behavior of inverted pendulum structures during earthquakes". *Bulletin of the Seismological Society of America*, **53**(2): 403-417. https://doi.org/10.1785/BSSA0530020403

2 Clough RW and Huckelbridge AA (1977). "*Preliminary Experimental Study of Seismic Uplift of a Steel Frame*". Report No. UCB/EERC-77/22, Earthquake Engineering Research Center, University of California, Berkeley.

3 Priestley MJN, Evison RJ and Carr AJ (1978). "Seismic response of structures free to rock on their foundations". *Bulletin of the New Zealand Society for Earthquake Engineering*, **11**(3): 141-150. https://doi.org/10.5459/bnzsee.11.3.141-150

4 Tilby C (1981). "South Rangitikei Railway Bridge Construction". *IPENZ Transactions*, **8**(2).

5 Frost G and Tilby C (2014). "South Rangitikei Railway Bridge - Construction engineering". *The New Zealand Concrete Steel Conference.* 9-11 October, Taupo, NZ.

6 Xiao Y, MacRae G, Hamada N, Priestley MJN and Seible F (1992). *"Rocking and Capacity Test of Model Bridge Pier"*. Structural Systems Research Project, Report No. SSRP 92/06, Department of Applied Mechanics and Engineering Sciences, University of California, San Diego.

7 Gledhill SM, Sidwell GK and Bell DK (2008). "The damage avoidance design of tall steel frame buildings - Fairlie Terrace Student Accommodation Project, Victoria University of Wellington". *Annual Conference of the New Zealand Society for Earthquake Engineering*, Paper # 63.

8 Bruneau M and MacRae G (2017). "*Reconstructing Christchurch: A Seismic Shift in Building Structural Systems*". QuakeCentre, University of Canterbury, NZ. https://resources.quakecentre.co.nz/reconstructing-christchurch/

9 Bruneau M and MacRae G (2019). "Building structural systems in Christchurch's post-earthquake reconstruction". *Earthquake Spectra*, **35**(4): 1953–1978. https://doi.org/10.1193/052818EQS126O

10 Deierlein G, Ma X, Hajjar F, Eatherton M, Krawinkler H, Takeuchi T, Midorikawa M, Hikino T and Kasai K (2010). "Seismic resilience of self-centering steel braced frames with replaceable energy-dissipating fuses; Part 2: E-Defense shake table test". *7th International Conference on Urban Earthquake Engineering & 5th International Conference on Earthquake Engineering Joint Conference,* 3-5 March, Tokyo.

11 Deierlein G, Ma X, Eatherton M, Hajjar JF, Krawinkler H, Takeuchi T, Kasai K and Midorikawa M (2011). "Earthquake resilient steel braced frames with controlled rocking and energy dissipating fuses". *Steel Construction Design and Research*, **4**(3): 171-175. https://doi.org/10.1002/stco.201110023

12 MacRae G (2013). "Low damage construction – Some system issues". *10th International Conference on Urban Earthquake Engineering*, 1-2 March, Tokyo Institute of Technology, Japan.

13 Wiebe L, Sidwell G and Gledhill S (2015). *"SCNZ: Design Guideline for Controlled Rocking Steel Braced Frames".* SCNZ Report 110. Prepared by Aurecon New Zealand Limited for SCNZ, NZ. https://www.scnz.org/wp-content/uploads/2020/11/P4_A-PRACTIONERS-GUIDE-TO-DESIGN-AND-DELIVERY-OF-CONTROLLED-ROCKING-STEEL-BRACED_Gledhill-min.pdf

14 Wiebe L (2015). "Controlled rocking steel braced frames: Connecting research and practice". *Steel Innovations Conference*, 3-4 September, Auckland, NZ.

15 Kordani R, Rodgers GW and MacRae GA (2017). "Effect of post-tensioning loss due to relaxation in structural rocking walls". *Annual Conference of the New Zealand Society for Earthquake Engineering*, 27-29 April, Wellington, NZ. https://www.nzsee.org.nz/db/2017/P1.31_Kordani.pdf

16 Rangwani K, MacRae GA, Rodgers GW, Soleimankhani H and J Cook (2020). "Tension-only device for a steel rocking frame system". *Proceedings of the New Zealand Society for Earthquake Engineering Annual Conference*, 22-24 April, Wellington, NZ.

17 Gledhill S (2015). *"*A practitioner's guide to design and delivery of controlled rocking steel braced frame structures". *Steel Innovations Conference*, Auckland, NZ.

18 Eatherton M, Hajjar J, Ma X, Krawinkler H and Deierlein G (2010). "Seismic design and behavior of steel frames with controlled rocking—Part I: Concepts and quasi-static subassembly testing". *NASCC and Structures Congress*, 12-15 May, Orlando, USA, pp.1523-1533. https://doi.org/10.1061/41130(369)138

19 Ma X, Krawinkler H and Deierlein GG (2011). "*Seismic design and behavior of self-centering braced frame with controlled rocking and energy dissipating fuses"*. Report No. 174, The John A. Blume Earthquake Engineering Center, Stanford University, Stanford, CA.

20 Royal Society Te Apārangi (2017). "*Buildings that better survive earthquakes*". Royal Society, Wellington, NZ. https://www.rnz.co.nz/national/programmes/ourchangingworld/audio/2018629110/buildings-that-better-survive-earthquakes

21 Rodgers GW, Chase JG and Mander JB (2019). "Repeatability and high-speed validation of supplemental lead-extrusion energy dissipation devices". *Advances in Civil Engineering*, 1–13. https://doi.org/10.1155/2019/7935026

22 Xie R, Chanchi GJ, MacRae GA, Chase G, Rodgers G and Clifton C (2015). "Hysteretic behaviour of a frame using a brace equipped with an asymmetrical friction connection (AFC)". *Steel Innovations Conference*, 3-4 September, Auckland, NZ.

23 MacRae GA and Clifton C (2015). "Research on seismic performance of steel structures in seismic areas". *STESSA Conference*, Tongji University, Shanghai, China.

24 MacRae GA (2020). "*Advanced Steel Structures*". ENEQ650 Lecture Notes, University of Canterbury, NZ.

25 Midorikawa M, Azuhata T, Ishihara T, Matsuba Y, Matsushima Y and Wada A (2002). "Earthquake response reduction of buildings by rocking structural systems". *Smart Structures and Materials 2002: Smart Systems for Bridges, Structures, and Highways.* 28 June, International Society for Optics and Photonics. **4696**: 265-272. https://doi.org/10.1117/12.472562

26 Midorikawa M, Azuhata T, Ishihara T and Wada A (2006). "Shaking table tests on seismic response of steel braced frames with column uplift". *Earthquake Engineering and Structural Dynamics*, **35**(14): 1767-1785. https://doi.org/10.1002/eqe.603

27 Wada A, Yamada S, Fukuta O and Tanigawa M (2001). "Passive controlled slender structures having special devices at column connections". *Seventh International Seminar on Seismic Isolation, Passive Energy Dissipation and Active Control of Vibrations of Structures*, 2-5 October, Assisi, Italy. http://akira-wada.com/00_img/article/2001/0102s01_7thInterSeminar200110Assisi.pdf

28 Tremblay R, Poirier LP, Bouaanani N, Leclerc M, Rene V, Fronteddu L and Rivest S (2008). "Innovative viscously damped rocking braced steel frames". *Proceedings of the 14th World Conference on Earthquake Engineering*, 12-17 October, Beijing, China.

29 Roke D, Sause R, Ricles J M and Gonner N (2009). "Damage-free seismic-resistant self-centering steel concentrically-braced frames". *STESSA2009*: *Proceedings of the 6th International Conference on Behaviour of Steel Structures in Seismic Areas*, 16-20 August, Philadelphia, Pennsylvania, USA. ISBN 10: 0203861590

30 Sause R, Ricles JM, Lin Y-C, Seo C-Y, Roke D and Chancellor B (2010). "Self-centring damage-free seismic-resistant steel frame systems". *7th International Conference on Urban Earthquake Engineering & 5th International Conference on Earthquake Engineering Joint Conference*, 3-5 March, Tokyo, Japan.

31 Eatherton M and Hajjar J (2011). "Residual drifts of self-centering systems including effects of ambient building resistance". *Earthquake Spectra*, **27**(3): 719-744. http://dx.doi.org/10.1193/1.3605318.

32 Wiebe L (2008). "*Mitigation of Higher Mode Effects in Self-Centring Walls by Using Multiple Rocking Sections*". Master of Earthquake Engineering Thesis, University Institute for Advanced Studies, University of Pavia, Italy.

33 Wiebe L (2013). "*Design of Controlled Rocking Steel Frames to Limit Higher Mode Effects*". PhD Thesis, University of Toronto, Toronto, Ontario, Canada.

34 Wiebe L, Christopoulos C, Tremblay R and Leclerc M (2013a). "Mechanisms to limit higher mode effects in a controlled rocking steel frame. 1: Concept, modelling, and low amplitude shake table testing". *Earthquake Engineering and Structural Dynamics*, **42**(7): 1053-1068. https://doi.org/10.1002/eqe.2259

35 Wiebe L, Christopoulos C, Tremblay R and Leclerc M (2013b). "Mechanisms to limit higher mode effects in a controlled rocking steel frame. 2: Large amplitude shake table testing". *Earthquake Engineering and Structural Dynamics*, **42**(7): 1069-1086. https://doi.org/10.1002/eqe.2258

36 Wiebe L and Christopoulos C (2014). "Performance-based seismic design of controlled rocking steel braced frames. I: Methodological framework and design of base rocking joint". *Journal of Structural Engineering*, 4014226. http://doi.org/10.1061/(ASCE)ST.1943-541X.0001202

37 MacRae G (1994). "P-Δ effects on single-degree-of-freedom structures". *Earthquake Spectra*, **10**(3): 539-568. http://dx.doi.org/10.1193/1.1585788

38 Gultom R and Ma QT (2015). "Biaxial pseudo dynamic tests of a post-tensioned rocking column with externally mounted energy dissipaters". *Proceedings of the NZSEE Annual Conference*, pp.429-436. Rotorua, NZ. http://hdl.handle.net/2292/26824.

39 Bagheri H, Hashemi A, Quenneville P, Yousef-beik SMM and Zarnani P (2019). "Experimental test of a new self-centring tension-only brace using the Resilient Slip Friction Joint". *11th Pacific Conference on Earthquake Engineering (PCEE)*, 4-9 April, Auckland, NZ. http://db.nzsee.org.nz/2019/Oral/4B.08%20Bagheri.pdf

40 Gunning M and Weston D (2013). "*Assessment of Design Methodology for Rocking Systems*". ENCN493 Project Report, Department of Civil and Natural Resources Engineering, University of Canterbury, Christchurch, NZ.

41 Cook J, Rodgers GW, MacRae GA and Chase JG (2015). "Experimentation with tension-only devices for use with seismic energy dissipation systems". *Proceedings of the Tenth Pacific Conference on Earthquake Engineering*, Sydney, Australia.

42 Cook J, Rodgers GW, MacRae GA and Chase JG (2015). "Development of a ratcheting, tension only fuse mechanism for seismic energy dissipation." *Proceedings of the New Zealand Society for Earthquake Engineering Annual Conference*, Rotorua, NZ.

43 Cook J, Rodgers GW, MacRae GA and Chase JG (2016). "Assessment of the structural response and cumulative displacement demand of Grip n' Grab tension-only bracing system". *Proceedings of the New Zealand Society for Earthquake Engineering Annual Conference*, Christchurch, NZ.

44 Cook J, Rodgers GW, MacRae GA and Chase JG (2017). "Testing and modelling of prototype tension-only seismic energy dissipation devices". *16th World Conference on Earthquake Engineering (16WCEE)*, Santiago, Chile.

45 Cook J, Rodgers GW and MacRae GA (2018). "Design and testing of ratcheting, tension-only devices for seismic energy dissipation systems". *Journal of Earthquake Engineering*, **24**: 1-22. http://doi.org/10.1080/13632469.2018.1441765

46 Cook J (2018). "*Design, Testing and Simulation of Grip 'n' Grab Ratcheting, Tension-only Devices for Seismic Energy Dissipation Systems*". PhD Thesis, University of Canterbury, Christchurch, NZ.

47 Cook J, Rodgers GW and MacRae GA (2019). "Assessment of cumulative inelastic displacement demand in energy dissipation systems using the Grip 'n' Grab tension-only mechanism*". Pacific Conference on Earthquake Engineering (PCEE)*, 4-6 April Auckland, NZ.

48 Rad A and MacRae G (2017). "Dynamically straightening of low-damage steel buildings after earthquakes". *16th World Conference on Earthquake Engineering (16WCEE)*, Santiago, Chile. https://www.wcee.nicee.org/wcee/article/16WCEE/WCEE2017-529.pdf

49 Anderson PM and Simcock DM (2015). *"Displacement Sensor"*. Final Year Project, University of Canterbury, Christchurch, NZ.

50 MacRae GA (2010). "Some steel seismic research issues". *Proceedings of the Steel Structures Workshop on Research Directions for Steel Structures*, University of Canterbury, Christchurch, NZ.

51 Livia E, Yoo J and MacRae GA (2019). "Development of a tension-only friction dissipater for rocking wall". *Pacific Conference on Earthquake Engineering (PCEE)*, 4-6 April Auckland, NZ.

52 Gu Z, Lu W and Ga Y (2022). "Asymmetrical friction damper to improve seismic behaviour of tension-only braces: An experimental and analytical study". *Engineering Structures*, **256**:114029. https://doi.org/10.1016/j.engstruct.2022.114029

53 Chanchi GJ, Xie R, MacRae GA, Chase G, Rodgers G and Clifton GC (2015). "Low damage brace using a symmetrical friction connection (SFC) detail". *New Zealand Society of Earthquake Engineering Annual Conference*, April, Rotorua, NZ.

54 Pall AS and Marsh C (1982). "Response of friction damped braced frames". *Journal of the Structural Division*, **108**(6): 1313–1323. http://palldynamics.com/pdf/40Pall_doc1.pdf

55 Grigorian CE and Popov EP (1994). "*Experimental and Analytical Studies of Steel Connections and Energy Dissipaters"*. Report UCB/EERC-95/13, Engineering Research Centre. San Francisco, USA.

56 Ramhormozian S, Clifton C and MacRae GA (2014). "The asymmetric friction connection with Belleville springs in the sliding hinge joint". *Proceedings of the New Zealand Society for Earthquake Engineering Annual Conference*, 21-23 March, Auckland, NZ. http://db.nzsee.org.nz/2014/poster/27_Ramhormozian.pdf

57 Ramhormozian S, Clifton C, MacRae GA and Davet GP (2017). "Stiffness-based approach for Belleville springs use in friction sliding structural connections". *Journal of Constructional Steel Research*, **138**: 340-356. https://dx.doi.org/10.1016/j.jcsr.2017.07.009

58 Chanchi JG, MacRae GA, Chase JG, Rodgers GW and Clifton GC (2016). "Effects of the bolt grip length on the behaviour of asymmetrical friction connections (AFC)". *Proceedings of the New Zealand Society for Earthquake Engineering Annual Conference*, NZ.

59 Chanchi JG, MacRae GA, Chase JG, Rodgers GW and Clifton GC (2020). "Asymmetric friction connection bolt lever arm effects on hysteretic behaviour". *Journal of Earthquake Engineering*, 1-22. http://dx.doi.org/10.1080/13632469.2020.1733136.

60 Hatami M, MacRae GA, Rodgers GW and Clifton C (2019). "Steel shim hardness effects on asymmetric friction connection performance". *12th Canadian Conference on Earthquake Engineering*, 17-20 June, Quebec, Canada.

61 Zhang R, Xie J-Y, Chouery K-E, Liu J-R, Jia L-J, Xiang P, Zhao X-Z, MacRae GA, Clifton GC, Dhakal RP, Ramhormozian S and Yan Z-D (2022). "Strong axis low-damage performance of rocking column-base joints with asymmetric friction connections". *Journal of Constructional Steel Research*, **191**: 107175. https://doi.org/10.1016/j.jcsr.2022.107175

62 Rangwani K, MacRae GA, Rodgers GW and Soleimankhani H (2021). "Rocking frame behaviour with tension only device – Numerical study". *Proceedings of the New Zealand Society for Earthquake Engineering (NZSEE) Annual Conference*, 12-16 April, Christchurch, NZ.

63 Soleimankhani H, MacRae G and Sullivan T (2021). "The oscillation resistance ratio (ORR) for understanding inelastic response". *Bulletin of the New Zealand Society for Earthquake Engineering*, **54**(3): 299-312. https://doi.org/10.5459/bnzsee.54.4.299-312

64 Newmark NM et al. (1948). "*Tentative Provisions for the Development of Seismic Regulations for Buildings*". Applied Technology Council Report ATC 3-06, NBS Special Publication 510, NSF Publication 78-8.

65 Berrill JB, Priestley MJN and Chapman HE (1980). "Section 2 - Design earthquake loading and ductility demand". *Bulletin of the New Zealand Society for Earthquake Engineering*, **13**(3): 232-241. https://doi.org/10.5459/bnzsee.13.3.232-241

66 Standards New Zealand (2016). "*NZS1170.5: Structural Design Actions - Part 5: Earthquake Actions - New Zealand Incorporating Amendment No. 1*". Standards New Zealand, Wellington, NZ. https://www.standards.govt.nz/shop/nzs-1170-52004

67 Vidic T, Fajfar P and Fischinger M (1994) "Consistent inelastic design spectra: Strength and displacement". *Earthquake Engineering and Structural Dynamics*, **23**(5): 507-521. https://doi.org/10.1002/eqe.4290230504

68 Rahgozar N, Moghadam A and Aziminejad A (2016). "Inelastic displacement ratios of fully self-centering-controlled rocking systems subjected to near-source pulse-like ground motions". *Engineering Structures*, **108**: 113-133. https://doi.org/10.1016/j.engstruct.2015.11.030

69 Joo A, Zsarnoczay A, Opoldusz M and Kollar L (2016). "Applicability of modal response spectrum analysis on rocking structures". *Proceedings of the 16th World Conference on Earthquake Engineering*, Santiago, Chile.

70 Seo CY (2005). *"Influence of Ground Motion Characteristics and Structural Parameters on Seismic Responses of SDOF Systems"*. PhD Thesis, Lehigh University, Bethlehem, PA.

71 Zhang C, Steele TC and Wiebe LDA (2018). "Design-level estimation of seismic displacements for self-centering SDOF systems on stiff soil". *Engineering Structures*, **177**: 431-443. https://doi.org/10.1016/j.engstruct.2018.09.067

72 Gulkan P and Sozen M (1974). "Inelastic responses of reinforced concrete structures to earthquake motions". *ACI Journal*, **71**(12): 604-610. https://doi.org/10.14359/7110

73 Applied Technology Council (1996). *"ATC 40 Seismic Evaluation and Retrofit of Concrete Buildings, Vol. 1 & 2"*. Report No. SSC 96-01. Applied Technology Council, Redwood City, California, USA. https://www.atcouncil.org/pdfs/atc40toc.pdf

74 Priestley MJN, Calvi MC and Kowalsky MJ (2007). *"Displacement-Based Seismic Design of Structures"*. IUSS PRESS, Pavia, Italy, 670pp.

75 FEMA (2000). "*FEMA356: Report on the Prestandard and Commentary for the Seismic Rehabilitation of Buildings*". Federal Emergency Management Agency, Washington, DC. https://www.nehrp.gov/pdf/fema356.pdf

76 Pennucci D, Sullivan TJ and Calvi GM (2011). "Displacement reduction factors for the design of medium and long period structures". *Journal of Earthquake Engineering*, **15**(S1): 1-29. https://doi.org/10.1080/13632469.2011.562073

77 MacRae GA, Zhao X, Clifton C, L-J Jia, Dhakal R, Xiang P, Ramhormozian S and Rodgers G (2020). "The China-NZ ROBUST friction building shaking table testing overview". *17th World Conference on Earthquake Engineering*, September, Sendai, Japan. Paper C000558.

78 Yan Z, Ramhormozian S, Clifton C. Bagheri H, Rangwani K, MacRae G, Quenneville P, Dhakal R, Xiang P, Jia L and Zhao X (2021). "Three-storey configurable steel framed building incorporating friction based energy dissipater: Structural configuration and instrumentation". *Proceedings of the New Zealand Society for Earthquake Engineering Annual Conference*, 14-16 April, Christchurch, NZ.

79 Rangwani K, MacRae GA, Rodgers GW, Yan Z, Clifton C and Ramhormozian S (2022). "Planning and prediction of large-scale ROBUST rocking frame test". *Draft Paper for Bulletin of the New Zealand Society for Earthquake Engineering.*

80 MacRae GA, Ahmadzadah S, Ashdown J, Soleimankhani H and McGann C (2021). *"*Moment frame column seismic demands*". Proceedings of the New Zealand Society for Earthquake Engineering Annual Conference*, 14-16 April, Christchurch, NZ.

81 McKenna F, Fenves GL and Scott MH (2003). "*Open System for Earthquake Engineering Simulation*". Pacific Earthquake Engineering Research Center, University of California, Berkeley, California. http://opensees.berkeley.edu

82 Rangwani et al (2018). "*ROBUST Outputs Folders".* https://www.dropbox.com/sh/h8x4zf03m02dj7y/AADmQfVa1c1EvSSqLRCtwY57a?dl=0.

83 Standards New Zealand (1997). *"NZS3404: Part 1. Steel Structures Standard, Part 1*". Standards Association of New Zealand, Wellington, NZ. https://www.standards.govt.nz/shop/nzs-3404-parts-1-and-21997

84 Carr A (2007). *"Ruaumoko Theory Manual: Volume 1*". https://doi.org/10.13140/RG.2.1.1872.2728

85 Jury RD (1978). "*Seismic Load Demands on Columns of Reinforced Concrete Multi-Storey Frames*". ME Thesis, University of Canterbury, Christchurch, 129pp.

86 Standards New Zealand (1982). *"NZS3101.1. 1982. Code of Practice for Design of Concrete Structures, Part 1*". Standards Association of New Zealand, Wellington, NZ. https://www.standards.govt.nz/shop/nzs-3101-11982/.

87 MacRae G and Carr A (1987). "Capacity design of steel moment resisting frames". *Pacific Conference of Earthquake Engineering (PCEE),* 4-6 April Auckland, NZ.